Electronic Supporting information for:

Heterocyclic arsinocarbynes *via* tandem transmetallation

Benjamin J. Frogley, Anthony F. Hill* and Ryan M. Kirk

Research School of Chemistry, Australian National University, Canberra, Australian Capital Territory, ACT 2601, Australia.

* Corresponding author. E-mail: a.hill@anu.edu.au

Author Contributions

BJF, RMK and AFH contributed equally to the conceptualization, experimental design, interpretation of experimental results and manuscript compilation. All experimental procedures and data acquisition, including structural analysis, were executed by BJF and RMK. AFH was responsible for overall project administration and direction.

General Experimental

Unless otherwise stated, experimental work including chromatography was carried out at room temperature under a dry and oxygen-free nitrogen atmosphere using standard Schlenk techniques with dried and degassed solvents.

NMR spectra were obtained on a Bruker Avance 400 (^{1}H at 400.1 MHz, ^{13}C at 100.6 MHz), a Bruker Avance 600 (^{1}H at 600.0 MHz, ^{13}C at 150.9 MHz), or a Bruker Avance 700 (^{1}H at 700.0 MHz, ^{13}C at 176.1 MHz) spectrometers at the temperatures indicated. Chemical shifts (δ) are reported in ppm with coupling constants given in Hz and are referenced to the proteo-impurity (^{1}H) or the deuterated solvent itself (^{13}C). The multiplicities of NMR resonances are denoted by the abbreviations s (singlet), d (doublet), t (triplet), m (multiplet), br (broad) and combinations thereof for more highly coupled systems. Where applicable, the stated multiplicity refers to that of the primary resonance exclusive of ^{183}W satellites. In some cases, distinct peaks were observed in the ^{1}H and ^{13}C{^{1}H} NMR spectra, but to the level of accuracy that is reportable (i.e. 2 decimal places for ^{1}H NMR, 1 decimal place for ^{13}C NMR) they are reported as having the same chemical shift. The abbreviation 'pz' is used to refer to the pyrazolyl rings on the Tp and Tp* ligands. Spectra provided generally correspond to samples obtained directly from chromatography and may contain residual solvent as recrystallised samples often display reduced solubility. Spectra include resonances in the region $4 < \delta_H < 5$ due to the BH protons. These signals are especially broad due to the quadrupolar nature of ^{10}/^{11}B nuclei, compromising the precision of both the chemical shift and associated integrals. Being remote from the metal, in our experience these are of limited diagnostic value and are not included in the experimental details below.

Infrared spectra were obtained using a Perkin-Elmer SpectrumOne FT-IR spectrometer. The strengths of IR absorptions are denoted by the abbreviations vs (very strong), s (strong), m (medium), w (weak), sh (shoulder) and br (broad). UV/Vis data were collected from solutions in 1 cm quartz cells using a PerkinElmer Lambda 465 spectrophotometer. Elemental microanalytical data were provided by the Elemental Microanalysis Service of Macquarie University. High-resolution electrospray ionisation mass spectrometry (ESI-MS) was performed by the ANU Research School of Chemistry mass spectrometry service with acetonitrile or methanol as the matrix.

Data for X-ray crystallography were collected with an Agilent SuperNova CCD diffractometer using Cu-Kα radiation (λ = 1.54184 Å) and the CrysAlis PRO software.[1] Data for complexes **3** and **4** were also collected at the Australian Synchrotron, part of ANSTO, using the MX2 beamline[2] and made use of the Australian Cancer Research Foundation (ACRF) detector, using silicon double crystal monochromated synchrotron radiation at 100 K. Raw frame data were collected using BluIce[3] and data reduction, interframe scaling, unit cell refinement and absorption corrections were processed using XDS.[4] The structures were solved by intrinsic phasing and refined by full-matrix least-squares on F^2 using the SHELXT and SHELXL programs.[5] Hydrogen atoms were generally located and refined using a riding model. Diagrams were produced using the CCDC visualisation program Mercury.[6]

Bromodiphenylarsine and 10-chloro-5,10-dihydrophenarsazinine were generously provided by Assoc. Prof. Geoffrey Salem. The complexes [W(≡CBr)(CO)$_2$(Tp*)],[7] [W(≡CSn^{n}Bu$_3$)(CO)$_2$(Tp*)][8] and [AuCl(SMe$_2$)][9] were prepared according to the literature methods. A modified version of a literature preparation of the methyl analogue was used to prepare 1-chloro-2,3,4,5-tetraphenylarsole.[10]

CAUTION: The arsenic compounds used herein are highly toxic and should only be handled in an efficient fume hood by suitably trained persons wielding the appropriate safety equipment.

Computational Details

Computational studies were performed by using the *SPARTAN18*® suite of programs.[11] Geometry optimisation (gas phase) was performed at the DFT level of theory using the exchange functional (ωBP97X-D) of Head-Gordon.[12] The Los Alamos effective core potential type basis set (LANL2Dζ) of Hay and Wadt[13] was used for W; the Pople 6-31G* basis sets[14] were used for all other atoms. Geometry optimisations were performed at the ωBP97X-D/6-31G*/LANL2Dζ level and frequency calculations were performed to confirm that the optimized structures were minima and to identify vibrational modes of interest.

Synthetic Procedures

Synthesis of [W(≡CAsPh$_2$)(CO)$_2$(Tp*)] (1). This compound was prepared previously in 66% yield from [W(≡CBr)(CO)$_2$(Tp*)] *via* lithiation followed by treatment with AsBrPh$_2$.[15] An alternative synthesis commencing instead from the corresponding stannylcarbyne is as follows. To a solution of [W(≡CSn^{n}Bu$_3$)(CO)$_2$(Tp*)] (500 mg, 0.596 mmol), AsBrPh$_2$ (185 mg, 0.599 mmol) and [AuCl(SMe$_2$)] (18 mg, 0.061 mmol) in toluene (20 mL) was warmed to 60 °C for 1 h, during which time the solution turned dark orange. After time this, the solution was cooled to RT and the volatiles were removed *in vacuo*. The residue was washed with *n*-pentane to remove most of the liberated tin by-products and the remaining residue was subjected to anaerobic column chromatography (50 x 3 cm silica gel column), eluting first with petroleum ether (40–60 °C) followed thereafter by 20% v/v CH_2Cl_2/petrol. A bright yellow/orange band was collected and the volatiles were removed under reduced pressure to give a flaky yellow-orange solid of pure **1** (380 mg, 0.488 mmol, 82%). Characterisational data were as previously published,[15] to which may be added: UV-Vis: λ_{max} (CH_2Cl_2)/nm = 420br (ε = 680 Lmol^{-1}cm^{-1}).

Synthesis of [W(≡CAsC$_{12}$H$_8$NH)(CO)$_2$(Tp*)] (2). *Method 1:* To a solution of [W(≡CBr)(CO)$_2$(Tp*)] (1.00 g, 1.59 mmol) in tetrahydrofuran (40 mL) at –78 °C was added *n*-butyllithium (1.6 M in THF, 1.0 mL, 1.6 mmol) at the mixture was stirred at reduced temperature for 30 min. After this time, 10-chloro-5,10-dihydrophenarsazinine (444 mg, 1.60 mmol) was added as a solid, the mixture warmed to RT and stirring was continued for 1 h. The volatiles were carefully removed *in vacuo*, and residue was extracted with CH_2Cl_2 and subjected to anaerobic column chromatography (50 x 4 cm silica gel column), eluting first with petroleum ether (40–60 °C) followed by 20% v/v CH_2Cl_2/petrol. A bright yellow band was collected and the volatiles removed under reduced pressure to give a bright yellow solid of pure **2** (260 mg, 0.329 mmol, 28%). A green-brown band follows shortly after and was identified as the non-classical vinylidene complex [W$_2$(μ-C$_2$H$_2$)(CO)$_4$(Tp*)$_2$] (*ca* 500 mg, 0.45 mmol, 57%) previously reported by Templeton[16] which results from dimerization of the tungsten methylidyne complex [W(≡CH)(CO)$_2$(Tp*)]. *Method 2*: A solution of [W(≡CSn^{n}Bu$_3$)(CO)$_2$(Tp*)] (1.00 g, 1.19 mmol), 10-chloro-5,10-dihydrophenarsazinine (331 mg, 1.19 mmol) and [AuCl(SMe$_2$)] (35 mg, 0.12 mmol) in toluene (50 mL) was warmed to 60 °C for 1 h, during which time the solution turned brown. Cooling, removal of the volatiles *in vacuo*, washing with *n*-pentane and finally chromatography under the same conditions as method 1 gave pure **2** (411 mg, 0.519 mmol, 44%). The non-classical vinylidene was again the only other major tungsten-containing product.

IR (CH_2Cl_2, cm^{-1}): 1980s, 1890s ν_{CO}. ^{1}H NMR (700 MHz, $CDCl_3$, 25 °C): 2.22 (s, 6 H, pzC*H$_3$*), 2.26 (s, 3 H, pzC*H$_3$*), 2.28 (s, 3 H, pzC*H$_3$*), 2.30 (s, 6 H, pzC*H$_3$*), 5.68 (s, 1 H, pzC*H*), 5.81 (s, 2 H, pzC*H*), 6.49 (s, 1 H, N*H*), 6.85 (d, $^3J_{HH}$ = 8.1, 2 H, AsC$_{12}$*H$_8$*NH), 6.94 (t', $^3J_{HH}$ = 7.3, 2 H, AsC$_{12}$*H$_8$*NH), 7.26 (t', $^3J_{HH}$ = 8.1, 2 H, AsC$_{12}$*H$_8$*NH), 6.94 (t', $^3J_{HH}$ = 7.5, 2 H, AsC$_{12}$*H$_8$*NH), 7.26 (t', $^3J_{HH}$ = 8.1, 2 H, AsC$_{12}$*H$_8$*NH), 7.55 (d, $^3J_{HH}$ = 7.5, 2 H, AsC$_{12}$*H$_8$*NH). ^{13}C{^{1}H} NMR (176 MHz, $CDCl_3$, 25 °C): 12.6, 12.7, 15.2, 16.5 (pz*C*H$_3$), 106.5, 106.6 (pz*C*H), 115.4, 118.6, 120.8, 130.1, 135.5, 142.1 (As*C$_{12}$*H$_8$NH), 144.5, 145.1, 152.0, 152.4 (pz*C*CH$_3$), 224.1 (*C*O, $^1J_{CW}$ = 169), 303.9 (W≡*C*, $^1J_{CW}$ = 184). MS (ESI, *m/z*): Found: 791.1384. Calcd for $C_{30}H_{31}As^{11}BN_7O_2{}^{184}W$ [M–e$^-$]$^+$: 791.1358. UV-Vis: λ_{max} (CH_2Cl_2)/nm = 419br (ε = 470 Lmol^{-1}cm^{-1}). Anal. Found: C, 45.53; H, 4.09; N, 12.00. Calcd for $C_{30}H_{31}AsBN_7O_2W$: C, 45.54; H, 3.95; N, 12.39%.

Crystals suitable for structure determination were grown by slow evaporation of a dichloromethane/*n*-hexane mixture at 4 °C. *Crystal data for* $C_{30}H_{31}BN_7O_2AsW$ (M_w =791.20 gmol^{-1}): triclinic, space group *P*-1 (no. 2), a = 10.5457(3), b = 10.9949(3), c = 14.6439(4) Å, α = 98.025(3)°, β = 95.841(2)°, γ = 115.100(3)°, V = 1497.81(8) Å^3, Z = 2, T = 150.0(1) K, μ(CuKα) = 8.702 mm^{-1}, D_{calcd} = 1.754 Mgm^{-3}, 17489 reflections measured (9.07° ≤ 2Θ ≤ 147.714°), 6058 unique (R_{int} = 0.0254, R_{sigma} = 0.0248) which were used in all calculations. The final R_1 was 0.0261 (I > 2σ(I)) and wR_2 was 0.0703 (all data) for 393 refined parameters without restraints. CCDC 2069506.

Synthesis of [W(≡CAsC$_4$Ph$_4$)(CO)$_2$(Tp*)] (3). A solution of [W(≡CSn^{n}Bu$_3$)(CO)$_2$(Tp*)] (500 mg, 0.596 mmol), 1-chloro-2,3,4,5-tetraphenylarsole (280 mg, 0.601 mmol) and [AuCl(SMe$_2$)] (18 mg, 0.061 mmol) in toluene (20 mL) was warmed to 60 °C for 1 h, during which time the ClAsC$_4$Ph$_4$ dissolved and the solution turned brown. After this time, the mixture was cooled to RT, the volatiles were removed *in vacuo*,

the residue was washed with *n*-pentane and finally subjected to anaerobic column chromatography (40 x 3 cm silica gel column), eluting first with petroleum ether (40–60 °C) followed by 30% v/v CH_2Cl_2/petrol. A yellow band was collected and the volatiles were removed under reduced pressure to give a green-yellow solid of pure **3** (266 mg, 0.271 mmol, 46%). This compound appears to be thermally sensitive and an anaerobic chloroform-d_1 solution was found (by ^{1}H NMR spectroscopic monitoring) to decompose into a mixture of unidentified products within a few hours at room temperature. Thus, rapid manipulation during synthesis and storage of the solid at low temperature is recommended.

IR (CH_2Cl_2, cm^{-1}): 1986s, 1894s ν_{CO}. ^{1}H NMR (700 MHz, $CDCl_3$, 25 °C): 2.26 (s, 3 H, pzC*H*$_3$), 2.28 (s, 3 H, pzC*H*$_3$), 2.36 (s, 6 H, pzC*H*$_3$), 2.38 (s, 6 H, pzC*H*$_3$), 5.69 (s, 1 H, pzC*H*), 5.86 (s, 2 H, pzC*H*), 6.88–6.92 (m, 4 H, AsC$_4$*Ph*$_4$), 7.02–7.08 (m, 12 H, AsC$_4$*Ph*$_4$), 7.20–7.26 (m, 4 H, AsC$_4$*Ph*$_4$). These phenyl resonances were partially obscured by impurities emerging from the rapid decomposition of the complex. ^{13}C{^{1}H} NMR (176 MHz, $CDCl_3$, 25 °C): 12.7, 12.8, 15.1, 16.9 (pz*C*H$_3$), 106.4, 106.7 (pz*C*H), 126.4, 126.5, 127.7, 127.9, 130.3, 130.4, 138.3, 139.0 (AsC$_4$*Ph*$_4$), 144.4, 145.1 (pz*C*CH$_3$), 147.1 150.0 (As*C*$_4$Ph$_4$), 151.9, 152.4 (pz*C*CH$_3$), 224.8 (*C*O, $^1J_{CW}$ = 169), 283.0 (W≡*C*, $^1J_{CW}$ = 199). MS (ESI, *m/z*): UV-Vis: λ_{max} (CH_2Cl_2)/nm = *ca* 347sh (ε = 11000 Lmol^{-1}cm^{-1}). This strong, broad absorbance likely obscures a weaker visible-region absorbance centred at *ca* 420–440 nm. Found: 981.2252. Calcd for $C_{46}H_{42}As^{11}BN_6O_2{}^{184}W$ [M+H]$^+$: 981.2274.

A crystal suitable for structure determination was grown by vapour diffusion of *n*-hexane into a chloroform solution at 4 °C and proved to be an *n*-hexane hemisolvate. *Crystal data for* $C_{49}H_{49}AsBN_6O_2W$ (M_w =1023.52 gmol^{-1}): monoclinic, space group *C*2/c (no. 15), *a* = 41.967(8), *b* = 10.063(2), *c* = 28.004(6) Å, *β* = 130.88(3)°, *V* = 8942(4) Å^3, *Z* = 8, *T* = 100.0(2) K, μ(Synchrotron) = 3.364 mm^{-1}, D_{calcd} = 1.521 Mgm^{-3}, 58300 reflections measured (2.908° ≤ 2Θ ≤ 52.742°), 8947 unique (R_{int} = 0.1159, R_{sigma} = 0.0646) which were used in all calculations. The final R_1 was 0.0552 ($I > 2\sigma(I)$) and wR_2 was 0.1571 (all data) for 552 refined parameters without restraints. CCDC 2076338.

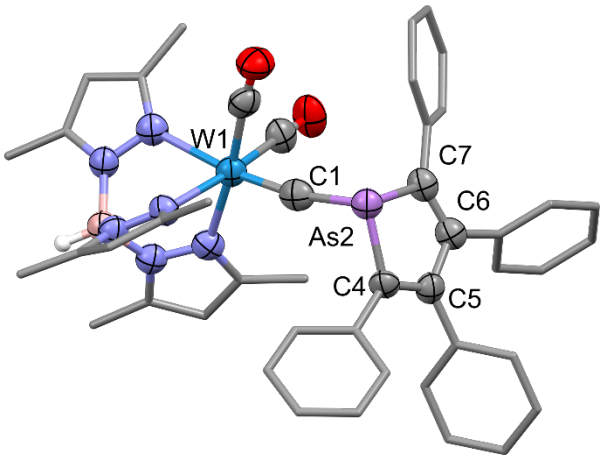

Figure S1. Molecular structure of **3** in a crystal of **3**·0.5C_6H_{14} showing 50% displacement ellipsoids. Pyrazolyl and phenyl rings are simplified and solvent is not shown for clarity. Selected distances [Å] and angles [°]: W1–C1 1.810(7), C1–As2 1.933(7), As2–C4 1.941(7), As2–C7 1.951(7), C4–C5 1.363(9), C5–C6 1.482(9), C6–C7 1.370(10), W1–C1–As2 167.9(4), C1–As2 C4 100.6(3), C1–As2–C7 99.4(3), C4–As2–C7 87.1(3), As2–C4–C5 109.9(5), C4–C5–C6 116.7(6), C5–C6–C7 115.3(6), C6–C7–As2 110.2(5).

A low-quality crystal of **7** was serendipitously obtained while attempting to grow crystals of **3** by slow evaporation of a dichloromethane and ethanol mixture. This structural model, which confirms connectivity, is included only as a point of interest as the data quality precludes interrogation of structural parameters. The structural model was not considered of sufficient precision for inclusion in the CCDC. *Crystal data for* $C_{96}H_{94}As_2B_2N_{12}O_7W_2$ (M_w =2066.99 gmol^{-1}): triclinic, space group *P*-1 (no. 2), *a* = 10.934(2), *b* = 12.172(2), *c* = 40.402(8) Å, *α* = 92.56(3)°, *β* = 92.94(3)°, *γ* = 116.20(3)°, *V* = 4805(2) Å^3, *Z* = 2, *T* = 100.0(2) K, μ(Synchrotron) = 3.134 mm^{-1}, D_{calc} = 1.429 Mgm^{-3}, 55489 reflections measured (1.012° ≤ 2Θ ≤ 52.744°), 17333 unique (R_{int} = 0.1248, R_{sigma} = 0.1295) which were used in all calculations. The final R_1 was 0.1360 ($I > 2\sigma(I)$) and wR_2 was 0.4351 (all data) for 1091 refined parameters with 739 restraints. Refinement of a structural model with the central oxygen replaced by methylene returned residuals R_1 = 0.1366 ($I > 2\sigma(I)$) and wR_2 = 0.4359 (all data) for 1091 refined parameters with 739 restraints. Accordingly, X-ray diffractometry does not ambiguously distinguish between the two possibilities, both of which should be considered mechanistically plausible.

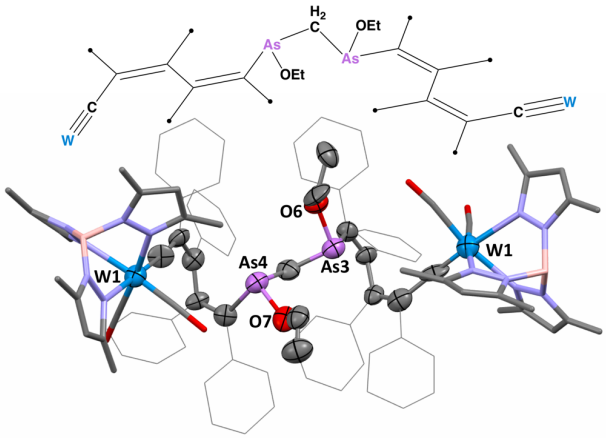

Figure S2. Molecular structure of **7** in a crystal (30% displacement ellipsoids, pyrazolyl and phenyl rings simplified; low precision structural model see ESI).

Synthesis of HC≡CAs(C$_6$H$_4$)$_2$NH (4).To a solution of 10-chloro-5,10-dihydrophenarsazinine (2.00 g, 7.22 mmol) in diethyl ether (100 mL) at 0 ˚C was added ethynylmagnesium bromide (0.5 M in tetrahydrofuran, 29 mL, 14.5 mmol). The mixture was warmed to RT and stirring continued for 3 h. The resulting green solution was quenched with saturated ammonium chloride (100 mL). The aqueous phase was extracted with diethyl ether, the extracts were washed with deionised water, dried over anhydrous magnesium sulfate, and the solvents were removed under reduced pressure. The residue was extracted with chloroform (10 mL), *n*-hexane was added (100 mL) and the $CHCl_3$ was removed under reduced pressure. The resulting precipitate was collected by filtration and washed with n-pentane (3 x 50 mL) to give a colourless microcrystalline solid of pure **4** (1.02 g, 3.82 mmol, 53%). ^{1}H NMR (400 MHz, $CDCl_3$, 25 °C): 2.35 (s, 1 H, C≡C*H*), 6.64 (br s, 1 H, N*H*), 6.88 (d, $^3J_{HH}$ = 8.1, 2 H, AsC$_{12}$H$_8$N), 7.00 (t', $^3J_{HH}$ = 7.7, $^4J_{HH}$ = 1.2, 2 H, AsC$_{12}$H$_8$N), 7.31 (t'd, $^3J_{HH}$ = 8.1, $^4J_{HH}$ = 1.2, 2 H,

$AsC_{12}H_8N$), 7.59 (dd, $^3J_{HH}$ = 7.5, $^4J_{HH}$ = 1.2, 2 H, $AsC_{12}H_8N$).^{1}H NMR (400 MHz, C_6D_6, 25 °C): 1.96 (s, 1 H, C≡C*H*), 5.88 (br s, 1 H, N*H*), 6.24 (d, $^3J_{HH}$ = 8.2, $^4J_{HH}$ = 1.0, 2 H, $AsC_{12}H_8N$), 6.75 (t', $^3J_{HH}$ = 7.3, $^4J_{HH}$ = 1.0, 2 H, $AsC_{12}H_8N$), 7.02 (t'd, $^3J_{HH}$ = 7.6, $^4J_{HH}$ = 1.5, 2 H, $AsC_{12}H_8N$), 7.42 (dd, $^3J_{HH}$ = 7.5, $^4J_{HH}$ = 1.4, 2 H, $AsC_{12}H_8N$). $^{13}C\{^1H\}$ NMR (101 MHz, $CDCl_3$, 25 °C): 84.6 (*C*≡CH), 88.8 (C≡*C*H), 114.7, 115.9, 121.6, 130.9, 134.8, 142.4 ($NC_{12}H_8As$). GC-MS (EI, *m/z*): Found: 265.9966. Calcd for $C_{14}H_9AsN$ $[M–H]^+$: 265.9945. Found: 267.0029. Calcd for $C_{14}H_{10}AsN$ $[M]^+$: 267.0024. MS (ESI, m/z): Found: 284.0060. Calcd for $C_{14}H_{10}AsNO$ $[M+O]^+$: 284.0056. Anal. Found: C, 62.92l H, 3.75; N, 5.08%. Calcd for $C_{14}H_{10}AsN$: C, 62.94; H, 3.77; N, 5.24%.

Crystals suitable for X-ray structure determination were grown by evaporation of a $CHCl_3$/*n*-hexane solution under reduced pressure. *Crystal data for* $C_{14}H_{10}NAs$ (M_w =267.15 $gmol^{-1}$): monoclinic, space group $P2_1/n$ (no. 14), a = 11.6500(3), b = 6.7526(2), c = 14.8906(4) Å, β = 102.826(2)°, V = 1142.18(6) Å^3, Z = 4, T = 150.0(1) K, μ(CuKα) = 3.757 mm^{-1}, D_{calcd} = 1.554 Mgm^{-3}, 3192 reflections measured (8.754° ≤ 2Θ ≤ 141.44°), 2108 unique (R_{int} = 0.0211, R_{sigma} = 0.0363) which were used in all calculations. The final R_1 was 0.0272 ($I > 2\sigma(I)$) and wR_2 was 0.0695 (all data) for 149 refined parameters without restraints. CCDC 2074686.

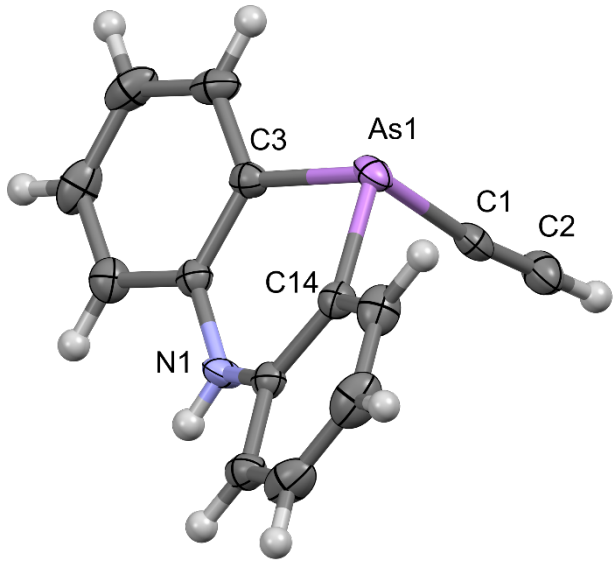

Figure S3. Molecular structure of **4** in a crystal showing 50% displacement ellipsoids. Selected distances [Å] and angles [°]: As1–C1 1.926(2), C1–C2 1.193(4), As1–C3 1.936(2), As1–C14 1.930(2), As1–C1–C2 172.1(2), C1–As1–C3 96.12(10), C1–As1–C14 97.46(9), C3–As1–C14 96.35(10).

Synthesis of HC≡CAsC_4Ph_4 (5). To a solution of 1-chloro-2,3,4,5-tetraphenyl-1*H*-arsole (1.20 g, 2.5 mmol) in THF (30 mL) a solution of Bu_3Sn(C≡CH) (0.97 g, 3.0 mmol, 1.2 equiv.) in THF (10 mL) was added *via* syringe, and the mixture heated to reflux for 90 minutes. During this time, the golden yellow colour discharges considerably. To the cooled mixture was added an aqueous solution of *ca* 0.5 g $KF{\cdot}2H_2O$ (in 25 mL water) and the mixture was then vigorously stirred overnight. After this time, volatiles were removed under reduced pressure and the residue extracted with CH_2Cl_2, partitioned from the aqueous phase, and filtered through a short Celite® plug (2 x 2 cm) to remove insoluble organotin-fluorides. The filtrate was washed again with dilute aqueous KF, then twice with water, and dried over anhydrous magnesium sulfate. Filtration and evaporation of the solvent provided a pale yellow residue which was purified by anaerobic flash chromatography on a short (20 x 3 cm) column of neutral alumina eluting with 9:1 *n*-pentane/CH_2Cl_2. A pale yellow band was collected and dried to give a tan-coloured solid which was re-crystallised from CH_2Cl_2/MeOH at -20 °C overnight providing of the title compound (0.705 g, 1.56 mmol, 60% isolated yield). A further *ca* 100 mg (7%) of slightly impure product was obtained upon concentrating the mother liquor. ^{1}H NMR (400 MHz, $CDCl_3$, 25 °C): δ_H = 2.78 (s, 1H, C≡C*H*), 7.03—7.08 (m, 8 H; AsC_4Ph_4), 7.13—7.20 (m, 12 H, AsC_4Ph_4).). $^{13}C\{^1H\}$ NMR (101 MHz, $CDCl_3$, 25 °C): δ_C = 80.0 (*C*≡CH), 94.1 (C≡*C*H), 127.0, 127.1, 127.9, 128.2, 129.5, 130.2, 137.3, 138.1, 146.9 (C_β), 151.3 (C_α). MS (EI, +ve ion, *m/z*) Found: 456.0859. Calcd for $C_{30}H_{21}{}^{75}As_1$ $[M]^+$: 456.0854. Single crystals suitable for X-ray diffractommetry were grown from CH_2Cl_2/MeOH at -20 °C. *Crystal data* for $C_{30}H_{21}As$ (M_w = 456.39 $gmol^{-1}$): monoclinic, space group $P2_1/c$ (no. 14), a = 19.0571(2) Å, b = 6.08720(10) Å, c = 20.2253(2) Å, β = 110.4510(10)°, V = 2198.34(5) Å^3, Z = 4, T = 150.0(1) K, μ(Cu-Kα) = 2.184 mm^{-1}, D_{calcd} = 1.379 Mgm^3, 13330 reflections measured (8.906° ≤ 2Θ ≤ 147.476°), 4440 unique (R_{int} = 0.0254, R_{sigma} = 0.0268) which were used in all calculations. The final R_1 was 0.0338 (I > 2σ(I)) and wR_2 was 0.0895 (all data). CCDC 2084057.

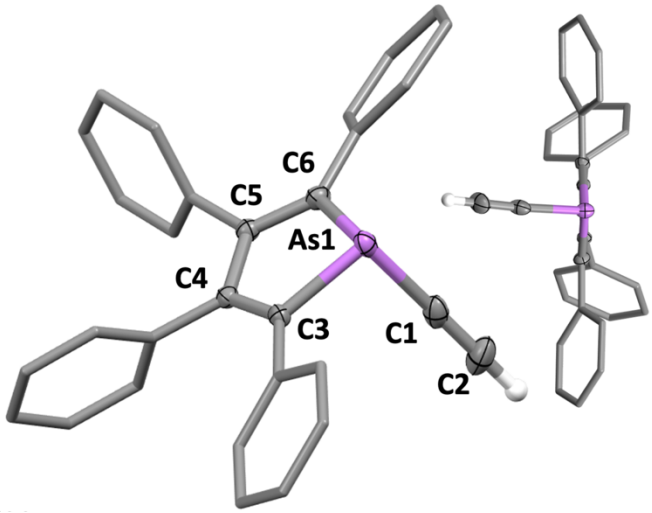

Figure S4. Molecular structures of HC≡CAsC_4Ph_4 (**5**) in crystals (50% displacement ellipsoids, aryl rings simplified). Selected distances [Å] and angles [°]: As1–C1 1.898(2), C1–C2 1.180(3), As1–C3 1.949(2), C3–C4 1.355(2), C4–C5 1.491(3), C5–C6 1.353(3), As1–C6 1.947(2), C1–As1–C3 96.00(9), C1–As1–C6 99.11(9), C3–As1–C6 87.17(8).

Geometry Optimisation of Model Compounds

In the interests of computational economy and visual simplicity model complexes involving a degree of atomic pruning were considered. The hydrotris(dimethyl-

pyrazolyl)borate (Tp*) ligand was replaced by the hydrotris(pyrazolyl)borate (Tp) ligand, which has a very modest effect on the electronic nature of the tungsten,[17] *e.g.*, [W(≡CC$_6$H$_4$Me-4)(CO)$_2$(L)] have ν_{CO} = 1986, 1903 cm^{-1} (L = Tp) and 1974, 1888 (L = Tp*), *i.e.*, $\Delta\nu \approx$ 12-15 cm^{-1}. We have on many occasions presented this simplification without justification and we therefore attend to this omission here. This was verified by interrogating the complexes [W(≡CAsPh$_2$)(CO)$_2$(L)] (L = Tp* **1**, Tp **1'**) at the same level of theory (DFT:ωBP97X-D/6-31G*/LANL2Dζ) from the perspectives of (i) geometry optimisation, (ii) vibrational frequencies (in particular ν_{CO} modes), (iii) Electronic spectra simulation (TD-DFT) and (iv) Natural charges.

(i) **Geometry:** The key geometric parameters associated with both the inner coordination sphere of tungsten and the WCAsC$_2$ spine of interest (Table S1) show remarkably little variation (< 0.3 % in distances; < 2% for angles) upon introduction of 3,5-methyl substituents on the pyrazolyl rings. These protrude between the remaining carbonyl and carbyne ligands thereby affording kinetic protection without perturbing the geometry.

Table S1. Calculated geometric parameters for [W(≡CAsPh$_2$)(CO)$_2$(L)]

Parameter	L= Tp*	L = Tp	Δ	%
	1	**1'**		
W≡C [Å]	1.802	1.801	0.001	0.1
W–CO [Å]	1.996	2.000		
	2.003 (2.000)[a]	2.008 (2.004)[a]	0.004	0.1
C–As [Å]	1.920	1.919	0.001	0.1
W–C–As [°]	171.67	173.93	2.26	1.3
W–N$_{trans}$ [Å]	2.350	2.350	0	0
W–N$_{cis}$ [Å]	2.234	2.229		
	2.241 (2.238)[a]	2.234 (2.232)[a]	0.006	0.3
OC–W–CO [°]	90.61	90.48	0.13	0.1
$^1/_3\Sigma$°NWN [°]	243.37 (81.12)[b]	240.13 (80.04)[b]	1.08	1.3
Σ°As [°]	293.4	293.1	0.3	0.1

[a] Average of two values. [b] Average of three values.

(ii) **Frequency Calculations:** As noted above, the Tp* ligand is a slightly stronger donor ligand than is the Tp ligand by virtue of the six methyl substituents.[17] Experimentally, this is typically manifest in ν_{CO} frequencies for complexes of the form [W(X)(CO)$_2$(L)] (X = a three-electron ligand, *e.g.*, CR, NO, C$_3$H$_5$) being 10-20 cm^{-1} lower for L = Tp* than for L = Tp. This trend is computationally reproduced here for complexes **1** and **1*** (Table S2) although the absolute calculated ν_{CO} frequencies for **1** (gas phase) are each somewhat higher ($\Delta\nu_s$ = 8 cm^{-1}, $\Delta\nu_{as}$ 30 cm^{-1}) than found experimentally for **1** (CH_2Cl_2 solution). The singular vibrational scaling factor for the ωBP97X-D/6-31G* combination is given as 0.949 by the National Institute of Standards and Technology (NIST),[18] as implemented in Spartan18. It would therefore appear that for complexes of this form for data in the ν_{CO} region of the infrared spectrum, a dual scaling factor[19] (ν > 1800 cm^{-1}: 0.940) is more prudent. Although it was not unambiguously identified in the experimental infrared spectrum of **1**,[17] the absorption corresponding primarily to the antisymmetric ν_{WCAs} mode was calculated to occur at 1108 cm^{-1} for **1'** and 1111/1107 cm^{-1} for **1**, essentially independent of Tp/Tp* substitution. The calculated intensities for thee modes are so low as to be unlikely to serve as experimentally diagnostic due to the low WC and CAs bond polarities.

Table S2. Selected calculated infrared frequencies for [W(≡CAsPh$_2$)(CO)$_2$(L)]

L =	Tp*	Tp*	Tp*	Tp	Tp
Parameter	**1**	**1**	**1**	**1'**	**1'**
	[Expt.]	[Calc.]	[Calc.][d]	[Calc.]	[Calc][d]
ν_{BH} [cm^{-1}]	2554	2478	2454	2434	2410
ν_{CO} [cm^{-1}]	1983	1991	1972	2004	1984
	1892	1922	1903	1937	1919
	(1938)[a]	(1957)[a]	1938	(1971)[a]	(1952)[a]
k_{CO}[b] [Ncm^{-1}]	15.14	15.44	15.14	15.66	15.36
ν_{WCAs} [cm^{-1}]	c	1107vw	1107vw	1108vw	1108vw

[a] Average of two values. [b] Cotton-Kraihanzel force constant. [c] Not unambiguously identified due to low WC and CAs bond polarities. [d] Harmonic frequency scaling factor = 0.940 for ν > 1800 cm^{-1}.

(iii) Electronic Spectra: Electronic transitions of interest are expected to be associated with metal to ligand charge transfer and accordingly, the increase in metal π-basicity evident above from vibrational spectroscopy upon Tp/Tp* substitution is expected to be manifest in the electronic spectra, not least because the HOMO is in all a cases a primarily metal-centred ("d_{xy}") orbital orthogonal to the W≡C bond. This increase in metal basicity due to an elevation of occupied metal orbitals would also appear to result in a comparable elevation of virtual orbitals such that the calculated electronic spectra for both complexes are essentially indistinguishable (Figure S4, Table S3).

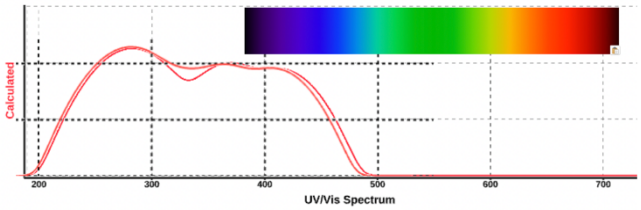

Figure S5. Superposition of calculated electronic spectra for [W(≡CAsPh$_2$)(CO)$_2$(L)] (L = Tp* **1**, Tp **1'**)

Table S3. Allowed transitions for electronic spectra for [W(≡CAsPh$_2$)(CO)$_2$(L)]

Transition	**Wavelength (intensity/ε** [L^{-1}mol^{-1}cm^{-1}]**)**		
	L = Tp (**1'**) [Calcd.]	Tp* (**1**) [Calcd.]	Tp* (**1**) [Exptl.]
HOMO-2 → LUMO+1 HOMO-3 → LUMO+1 HOMO → LUMO+9 HOMO → LUMO+2	278.83 (0.005)	272.43 (0.011)	
HOMO → LUMO+2 HOMO-2 → LUMO+1 HOMO → LUMO+9	284.27 (0.021)	283.79(0.023)	
HOMO-1 → LUMO+1 HOMO-2 → LUMO	292.87 (0.011)	288.47(0.007)	
HOMO-1 → LUMO HOMO-2 → LUMO	320.83 (0.005)	325.32 (0.005)	
HOMO → LUMO+1	374.69 (0.008)	364.16 (0.009)	
HOMO → LUMO	410.36 (0.005)	407.90 (0.007)	420 (ε = 680)

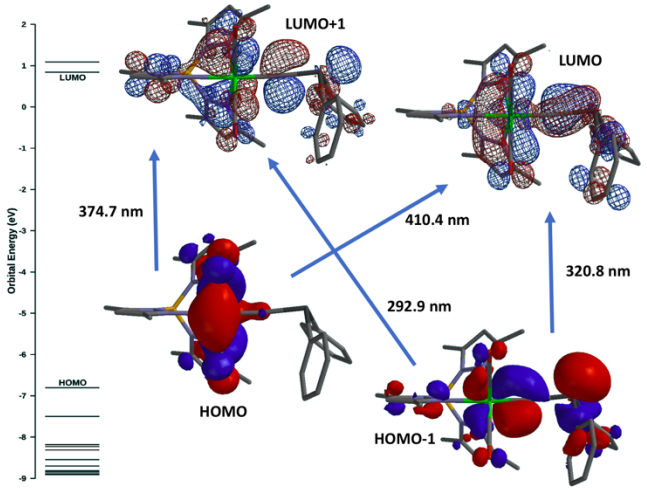

Figure S6. Frontier orbitals of relevance to electronic spectra.

In both cases the observed colour arises from a combination of HOMO→LUMO and HOMO→LUMO+1 transitions (Figure S5). Both of these involve charge transfer from the 'd_{xy}' orbital associated with W–CO π-bonding (retrodonation) to one of two orbitals that have W≡C π-antibonding character. Of these, the LUMO+1 includes a considerable contribution from arsenic.

(iv) Natural Charges and Bond Orders: Table S4 collates selected natural Lowden charges and bond orders associated with the W≡C–As spine calculated for both **1** and **1'**. It can be seen that the differences in each of these parameters is negligible.

Table S4. Natural charges and Löwden bond orders calculated for [W(≡CAsPh$_2$)(CO)$_2$(L)]

	L = Tp* (**1**)	L = Tp (**1'**)	Δ
Charge			
W	+1.006	+0.976	0.030
C	–0.674	–0.659	0.015
As	+0.939	+0.940	0.001
C(CO)[a]	+0.397	+0.401	0.004
N_{trans}	–0.410	–0.403	0.007
Löwdin Bond Order			
W≡C	2.506	2.526	0.020
C–As	1.028	1.034	0.006
W–CO[a]	1.369	1.356	0.013
W–N_{trans}	0.569	0.560	0.009

[a] Average of two values

These observations (i) – (iv) taken together would appear to indicate that for computational purposes, the Tp ligand is a reasonable, cost-effective substitute for the Tp* ligand in that the geometry of the coordination sphere is not significantly perturbed and the impact on metal π-basicity evident from IR data, whilst significant, is predictably consistent

In consideration of arsoles **3** and **5**, we note that the experimentally determined structures involve the phenyl substituents lying out of the arsole plane, *i.e.*, they are not conjugated and it is therefore reasonable to replaced them with non-mesomeric hydrogen substituents in **3'** and **5'**. We expect that these simplifications do not impact dramatically on the emerging conclusions. The potential impact of conjugation upon the arsole ring was, however, considered with reference to the 9-arsa-fluorenyl substituent in for [W{≡CAs(C$_6$H$_4$)$_2$}(CO)$_2$(L)] (**6'**) for which the dibenzo substitution effectively reduces the aromaticity of the arsole ring.

Catersian Coordinates for Optimised Geometries (ωBP97X-D/6-31G*/LANL2Dζ)

(a) [W(≡CAsPh$_2$)(CO)$_2$(Tp)] (1')

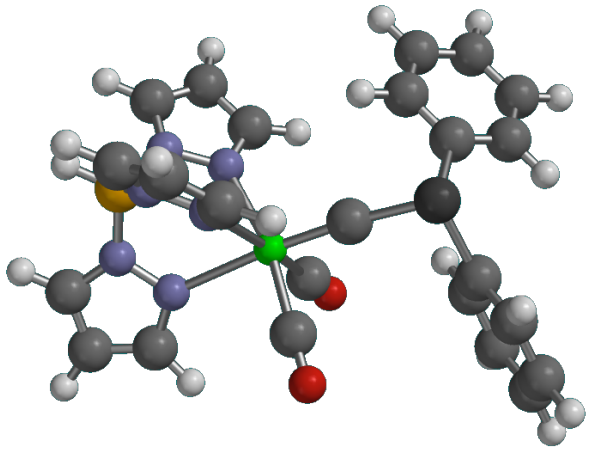

Figure S7. Optimised geometry for **1'** (ωBP97X-D/6-31G*/LANL2Dζ)

Table S5. Cartesian Coordinates for **1'**.

Atom	x	y	z
W	0.609232	-0.547061	0.734565
As	-0.301310	2.895747	-0.321633
N	-0.750187	-1.706941	3.356667
N	-0.243129	-0.586424	2.799130
N	-1.526270	-2.824456	1.264028
O	1.741576	-1.037039	-2.170476
N	0.703359	-3.417737	2.243885
N	-1.133318	-1.888803	0.371856
O	3.303069	0.861938	1.602816
C	0.083431	1.086075	0.186797
N	1.474692	-2.591122	1.505052
C	1.341065	-0.857597	-1.100968
C	-1.006337	-0.089195	4.846516
H	-1.261537	0.458692	5.740093
C	2.324317	0.338803	1.286647
C	-0.391985	0.395784	3.689111
C	-2.592469	-3.486899	0.785118
C	-1.214298	-1.432289	4.587888
C	-2.911615	-2.969077	-0.458256
H	-3.712597	-3.273579	-1.113673
C	-2.525295	1.478708	-1.562869
H	-2.566339	0.947232	-0.615087
C	1.719298	2.399904	-2.420544
C	1.401490	-4.516905	2.576310
C	2.673130	-4.408985	2.041190
H	3.484195	-5.116238	2.118329
C	-1.959357	-1.970511	-0.673101
C	1.342722	3.203989	-1.340073
C	2.664858	-3.178124	1.378618
C	-2.428138	2.814767	-3.998895
H	-2.384119	3.339059	-4.949301
C	-1.537346	2.443098	-1.780219
C	2.187387	4.235742	-0.929344
H	1.905661	4.866849	-0.089993
C	-1.501417	3.115050	-3.002910
C	2.923707	2.627173	-3.076596
H	3.210938	1.990876	-3.908249
B	-0.752550	-3.037810	2.582512
C	-3.450297	1.178819	-2.558603
H	-4.208850	0.421825	-2.378919
C	-3.402285	1.845151	-3.780867
H	-4.121757	1.610445	-4.559825
C	3.764812	3.657634	-2.658937
H	4.708931	3.828499	-3.167773
C	3.396193	4.461885	-1.585905
H	4.048316	5.265024	-1.255490
H	-1.271358	-3.905721	3.235880
H	3.448202	-2.687234	0.818235
H	0.942959	-5.295219	3.168383
H	-1.657051	-2.212769	5.188718
H	-0.053978	1.392053	3.443664
H	-1.826236	-1.304255	-1.513674
H	-3.043605	-4.279899	1.362960
H	1.068947	1.596340	-2.751410
H	-0.737456	3.864729	-3.191381

Thermodynamic properties (298.15 K): *ZPE* = 1019.21 kJmol^{-1}, H^o = –3733.121761 au, S^o = 910.12 Jmol^{-1}K^{-1}, G^o = –3733.225114, C_v = 518.71 Jmol^{-1}K^{-1}.

Table S6. Allowed transitions for electronic spectra. (ωBP97X-D/6-31G*/LANL2Dζ(W))

nm	Strength	Transition	%
278.8	0.0053	HOMO-2 → LUMO+1	31
		HOMO → LUMO+9	14
		HOMO → LUMO+2	12
284.3	0.0205	HOMO → LUMO+2	34
		HOMO-2 → LUMO+1	19
		HOMO → LUMO+9	18
292.9	0.0111	HOMO-1 → LUMO+1	39
		HOMO-2 → LUMO	24
320.8	0.0053	HOMO-1 → LUMO	63
		HOMO-2 → LUMO	13
374.7	0.0077	HOMO → LUMO+1	82
410.4	0.0047	HOMO → LUMO	89

(b) [W(≡CAsPh$_2$)(CO)$_2$(Tp*)] (1)

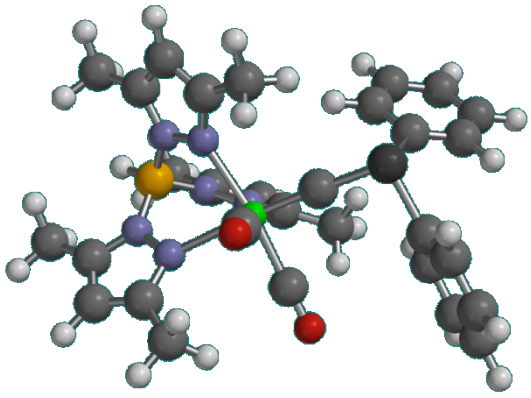

Figure S8. Optimised geometry for **1** (ωBP97X-D/6-31G*/LANL2Dζ)

Table S5. Cartesian Coordinates for **1**.

Atom	x	y	z
W	0.970104	0.158685	0.427422
As	0.376093	3.596798	-0.838750
N	-0.894077	-1.109900	2.642307
N	-0.348964	0.063271	2.227809
N	-1.107662	-2.225364	0.416897
O	2.829110	-0.222429	-2.098585
N	0.877824	-2.728507	1.877966
N	-0.592865	-1.238200	-0.363625
O	3.258230	1.710597	1.943434
C	0.568846	1.781438	-0.245303
N	1.768232	-1.856349	1.337049
C	2.156816	-0.088955	-1.167531
C	-1.597345	0.442449	4.038952
H	-2.089788	0.947979	4.856731
C	2.428068	1.124670	1.389021
C	-0.767927	1.016775	3.069299
C	-2.017200	-2.937469	-0.277661
C	-1.652979	-0.907051	3.737875
C	-2.093167	-2.391694	-1.547057
H	-2.723519	-2.719866	-2.360591
C	-2.335433	2.536298	-1.106233
H	-2.112574	2.019928	-0.175426
C	1.409426	2.575719	-3.416733
C	1.522340	-3.808236	2.364300
C	2.874640	-3.626598	2.129110
H	3.677189	-4.301167	2.390079
C	-1.180883	-1.331403	-1.562706
C	1.578005	3.501109	-2.383346
C	2.985518	-2.390373	1.482762
C	-2.900566	3.774593	-3.531382
H	-3.114335	4.256831	-4.480993
C	-1.355052	3.317112	-1.726463
C	2.675859	4.362664	-2.412391
H	2.818754	5.087114	-1.614338
C	-1.650681	3.941226	-2.939804
C	2.326289	2.511110	-4.459311
H	2.190571	1.781480	-5.252195
B	-0.630135	-2.413571	1.868300
C	-3.584055	2.371030	-1.698298
H	-4.330880	1.750442	-1.211599
C	-3.869244	2.989281	-2.913063
H	-4.842154	2.857350	-3.377326
C	3.422373	3.371326	-4.479902
H	4.140919	3.316348	-5.292402
C	3.596159	4.297783	-3.457184
H	4.448811	4.970384	-3.468614
H	-1.232079	-3.315211	2.379717
H	0.557764	1.903518	-3.405097
H	-0.897852	4.544349	-3.440679
C	0.822860	-4.952215	3.024492
H	1.557001	-5.698921	3.335698
H	0.111166	-5.432933	2.345943
H	0.267282	-4.627871	3.909935
C	4.230207	-1.717887	0.998529
H	5.099523	-2.337898	1.231501
H	4.371562	-0.742380	1.472457
H	4.204852	-1.560033	-0.083453
C	-2.759710	-4.098999	0.298899
H	-2.077964	-4.895969	0.612057
H	-3.440064	-4.506508	-0.452554
H	-3.349383	-3.806511	1.173431
C	-2.384025	-2.004442	4.440958
H	-1.697887	-2.775398	4.805465
H	-3.108924	-2.491952	3.781573
H	-2.922567	-1.593106	5.297828
C	-0.383708	2.451911	2.928866
H	0.700380	2.572881	2.859391
H	-0.743926	3.018851	3.790985
H	-0.817779	2.889639	2.024123
C	-0.863356	-0.416249	-2.697359
H	0.194549	-0.475728	-2.969467
H	-1.084779	0.621212	-2.432718
H	-1.461838	-0.686808	-3.571023

Thermodynamic properties (298.15 K): *ZPE* = 1440.55 kJmol^{-1}, H^o = –3968.822957 au, S^o = 1076.04 Jmol^{-1}K^{-1}, G^o = –3968.945152, C_v = 670.13 Jmol^{-1}K^{-1}.

Table S8. Allowed transitions for electronic spectra. (ωBP97X-D/6-31G*/LANL2DζW))

nm	Strength	Transition	%
272.4	0.0114	HOMO-3 → LUMO+1	37
		HOMO-2 → LUMO+1	16
283.8	0.0226	HOMO → LUMO+9	33
		HOMO → LUMO+2	18
288.5	0.0070	HOMO-1 → LUMO+1	31
		HOMO-3 → LUMO	19
		HOMO → LUMO+9	11
325.3	0.0050	HOMO-1 → LUMO	71
364.2	0.0089	HOMO → LUMO+1	80
407.9	0.0066	HOMO → LUMO	87

(c) [W{≡CAs{C_6H_4)$_2$NH}(CO)$_2$(Tp)] (2*)

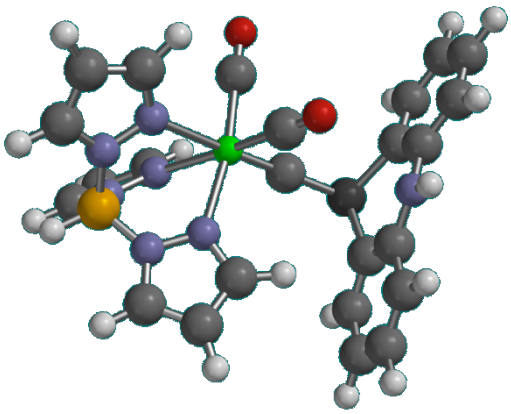

Figure S9. Optimised geometry for **2'** (ωBP97X-D/6-31G*/LANL2Dζ)

Table S6. Cartesian Coordinates for **2'**.

Atom	x	y	z
W	0.337076	0.730935	0.882847
As	-3.078986	-0.284283	-0.206931
N	1.703370	-0.741699	3.338390
N	0.567099	-0.135667	2.930424
N	2.462692	-1.611267	1.128473
O	0.674065	1.973465	-1.999090
N	3.382974	0.552950	2.001451
N	1.451679	-1.131359	0.370882
O	-0.868832	3.451049	1.956989
N	-1.792324	0.422434	-3.05361
C	-1.330084	0.249535	0.408678
N	2.537080	1.404507	1.383239
C	0.540791	1.520199	-0.943567
C	0.284680	-0.850486	5.035333
H	-0.157297	-1.054685	5.997996
C	-0.416835	2.464763	1.561641
C	-0.294898	-0.194669	3.946600
C	2.904969	-2.770446	0.610745
C	1.556809	-1.178488	4.600512
C	2.160745	-3.059568	-0.519119
H	2.251473	-3.914409	-1.170804
C	-2.319707	-2.831075	-1.361854
H	-2.778116	-3.230301	-0.460343
C	-2.643180	1.405088	-2.556973
C	4.578808	1.141296	2.173030
C	4.517987	2.421418	1.650348
H	5.302092	3.162003	1.623988
C	1.260741	-1.996380	-0.626274
C	-3.359662	1.252252	-1.361108
C	3.211266	2.533995	1.166625
C	-1.127642	-1.803100	-3.640387
H	-0.667304	-1.403104	-4.540979
C	-2.365464	-1.455106	-1.588763
C	-4.214521	2.272717	-0.941885
H	-4.772854	2.145440	-0.017501
C	-1.775753	-0.930872	-2.751082
C	-2.774990	2.595606	-3.285759
H	-2.215358	2.722121	-4.209570
B	2.918709	-0.864479	2.395509
C	-1.676723	-3.693406	-2.242550
H	-1.639459	-4.758532	-2.039693
C	-1.073380	-3.164884	-3.381921
H	-0.561827	-3.817816	-4.082990
C	-3.608453	3.608145	-2.837389
H	-3.688785	4.524273	-3.414877
C	-4.344723	3.451498	-1.664944
H	-5.002562	4.240378	-1.315583
H	3.811889	-1.460997	2.939222
H	-1.269251	0.687009	-3.874098
H	0.488491	-1.810717	-1.358664
H	3.716703	-3.301995	1.084999
H	5.384904	0.607347	2.654374
H	2.722811	3.364256	0.675831
H	-1.279909	0.233971	3.833527
H	2.368974	-1.688857	5.096660

Thermodynamic properties (298.15 K): *ZPE* = 1008.90 kJmol^{-1}, H^o = –3787.275599 au, S^o = 884.91 Jmol^{-1}K^{-1}, G^o = –3387.376089, C_v = 524.21 Jmol^{-1}K^{-1}.

Table S7 Allowed transitions for electronic spectra. (ωBP97X-D/6-31G*/LANL2Dζ(W))

nm	Strength	Transition	%
282.5	0.0176	HOMO → LUMO+3	26
		HOMO-3 → LUMO+1	16
		HOMO → LUMO+2	11
		HOMO → LUMO+9	11
292.4	0.0081	HOMO-3 → LUMO	32
		HOMO-2 → LUMO+1	27
		HOMO-3 → LUMO	13
299.3	0.0238	HOMO-1 → LUMO	66
326.1	0.0018	HOMO-2 → LUMO	75
374.3	0.0070	HOMO → LUMO+1	81
419.8	0.0043	HOMO → LUMO	85

(d) [W(≡CAsC$_4$H$_4$)(CO)$_2$(Tp)] (3')

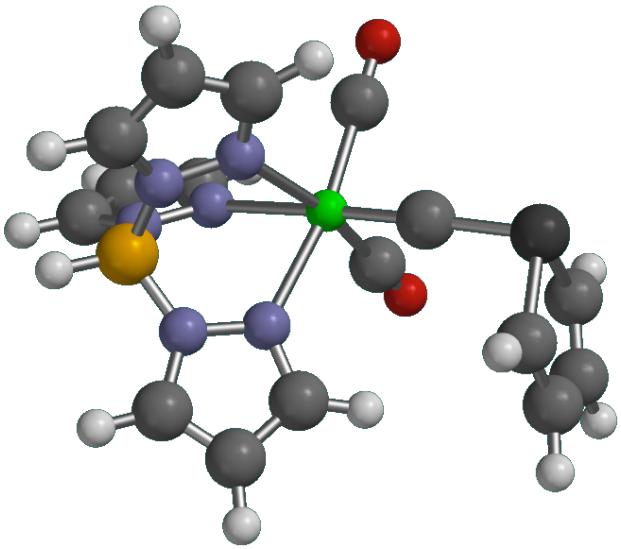

Figure S10. Optimised geometry for **3'** (ωBP97X-D/6-31G*/LANL2Dζ)

Table S8. Cartesian Coordinates for **3'**

Atom	x	y	z
W	0.444332	0.988111	-0.183841
As	3.935217	0.653530	1.035888
N	-2.125746	0.367357	1.545680
N	-0.943998	1.024612	1.551635
N	-0.211709	-1.134380	-0.198204
N	-2.666659	0.518957	-0.904680
O	0.821864	4.131365	-0.125122
N	-1.493443	-1.505010	0.015899
C	2.092367	0.811855	0.508602
N	-1.581220	1.217483	-1.305764
O	1.872194	0.723873	-2.994871
C	0.499173	-2.250441	-0.378680
C	-3.307599	1.731335	-2.648599
H	-3.899653	2.176093	-3.437151
C	-1.952743	1.341744	3.532202
H	-2.154895	1.674866	4.541258
C	-1.955358	1.952582	-2.355970
C	3.937870	-1.273380	1.266689

Atom	x	y	z
C	-2.750990	0.546044	2.724410
C	-1.592587	-2.847313	-0.030044
C	-3.716162	0.810341	-1.695523
C	-0.828850	1.617326	2.743219
C	4.677889	0.309872	-0.722120
C	1.340069	0.833756	-1.975779
C	-0.334578	-3.372754	-0.281826
H	-0.060371	-4.414590	-0.380179
C	4.529662	-1.880482	0.221374
C	4.938906	-0.999170	-0.887628
C	0.679852	2.985496	-0.160253
B	-2.578752	-0.442828	0.305847
H	-3.646560	-0.965799	0.507795
H	-1.235961	2.600447	-2.844244
H	-4.677115	0.342033	-1.521827
H	0.054839	2.203330	2.965149
H	-3.718876	0.093824	2.901254
H	1.566772	-2.180876	-0.552994
H	-2.551143	-3.328037	0.120276
H	4.699536	-2.956555	0.171054
H	3.575740	-1.780661	2.156579
H	4.908937	1.084458	-1.448025
H	5.409747	-1.408416	-1.781488

Thermodynamic properties (298.15 K): *ZPE* = 726.49 kJmol^{-1}, H^o = –3424.829650 au, S^o = 743.70 Jmol^{-1}K^{-1}, G^o = –3424.914104, C_v = 403.70 Jmol^{-1}K^{-1}.

Table S9 Allowed transitions for electronic spectra. (ωBP97X-D/6-31G*/LANL2Dζ(W))

nm	Strength	Transition	%
273.1	0.0071	HOMO → LUMO+1	50
		HOMO → LUMO+2	12
285.3	0.0259	HOMO → LUMO+3	31
		HOMO → LUMO+6	23
		HOMO → LUMO+1	11
289.8	0.0008	HOMO-2 → LUMO	27
		HOMO-1 → LUMO+2	22
		HOMO → LUMO+3	12
322.8	0.0010	HOMO-1 → LUMO	68
369.2	0.0098	HOMO → LUMO+2	68
		HOMO → LUMO+1	17
413.9	0.0060	HOMO → LUMO	86

(d) [W{≡CAs(C_6H_4)$_2$}(CO)$_2$(Tp)] (6')

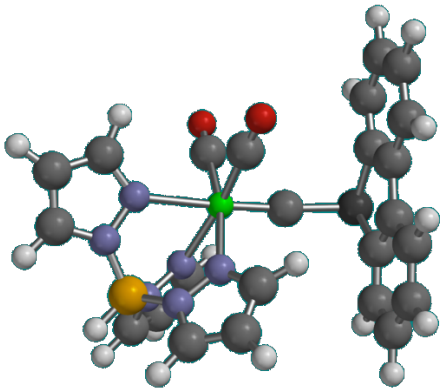

Figure S11. Optimised geometry for **6'** (ωBP97X-D/6-31G*/LANL2Dζ)

Table S10. Cartesian Coordinates for **6'**.

Atom	x	y	z
W	0.785832	1.141135	-0.021682
As	-0.286427	-0.192424	-3.322599
N	-0.975457	3.188119	1.638141
N	-0.439780	2.954654	0.420106
N	-1.261462	0.821085	2.378626
O	2.562783	-1.470292	-0.020430
N	0.771482	2.110594	3.076105
N	-0.759855	0.207872	1.284375
O	3.063813	2.789519	-1.467918
C	0.221840	0.596811	-1.640720
N	1.617236	1.698624	2.106311
C	1.926895	-0.507523	-0.019452
C	-1.601446	4.868641	0.338353
H	-2.050562	5.780697	-0.022576
C	2.237580	2.187614	-0.928792
C	-0.809885	3.962704	-0.371215
C	-2.198105	0.040540	2.945322
C	-1.676845	4.333644	1.612588
C	-2.314385	-1.119369	2.200414
H	-2.972913	-1.955766	2.375004
C	-2.763371	-1.336996	-2.069635
H	-3.269482	-0.392904	-2.250210
C	0.628591	-2.766686	-2.676280
C	1.459751	2.380677	4.198240
C	2.801423	2.139753	3.959299
H	3.625362	2.258483	4.645681
C	-1.383706	-0.965332	1.169961
C	1.087014	-1.578885	-3.267985
C	2.843856	1.713939	2.628358
C	-1.457728	-3.761209	-1.575214
H	-0.961964	-4.706727	-1.374800
C	-1.444178	-1.516175	-2.466428
C	2.396495	-1.467154	-3.717151
H	2.748089	-0.542385	-4.166296
C	-0.777178	-2.728955	-2.223166
C	1.504585	-3.844226	-2.544746
H	1.172070	-4.772854	-2.089768
B	-0.745530	2.207720	2.806279
C	-3.431856	-2.371770	-1.417989
H	-4.459833	-2.235270	-1.096343
C	-2.778369	-3.578504	-1.174790
H	-3.300674	-4.384655	-0.668008
C	2.815432	-3.731628	-2.995444
H	3.494310	-4.572136	-2.887918
C	3.264312	-2.547708	-3.576883
H	4.291274	-2.465311	-3.919497
H	-1.323122	2.587941	3.791084
H	3.688688	1.417942	2.022469
H	0.945290	2.724068	5.083680
H	-2.175160	4.685702	2.503668
H	-0.489112	3.975171	-1.402555
H	-1.135757	-1.628885	0.354200
H	-2.709863	0.368081	3.838225

Thermodynamic properties (298.15 K): *ZPE* = 766.14 kJmol^{-1}, H^o = –3731.965790 au, S^o = 855.71 Jmol^{-1}K^{-1}, G^o = –3732.053963, C_v = 504.08 Jmol^{-1}K^{-1}.

Table S11 Allowed transitions for electronic spectra for **6'**.

nm	Strength	Transition	%
277.7	0.0061	HOMO-3 → LUMO+2	33
283.9	0.0170	HOMO → LUMO+4	47
		HOMO → LUMO+8	23
291.2	0.006	HOMO-3 → LUMO	28
		HOMO-1 → LUMO+2	21
		HOMO-2 → LUMO	11
326.0	0.0025	HOMO-1 → LUMO	56
		HOMO-2 → LUMO	19
369.4	0.0079	HOMO → LUMO+2	73
421.9	0.0047	HOMO → LUMO	89

(e) HC≡CAs{C_6H_4)$_2$NH (4)

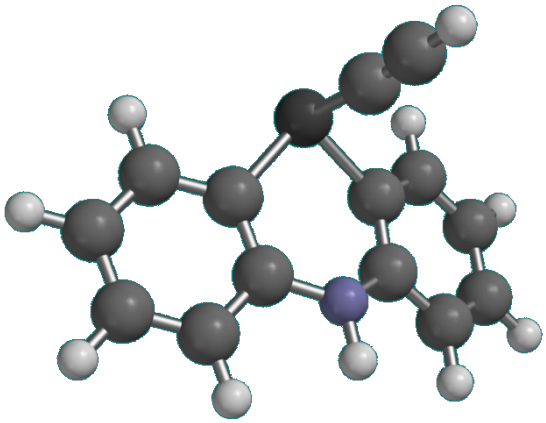

Figure S12. Optimised geometry for **4** (ωBP97X-D/6-31G*)

Table S12. Cartesian Coordinates for **4**

Atom	x	y	z
As	-0.369639	1.929794	0.388129
N	0.376070	-1.067569	-0.440038
C	1.074646	-0.601607	0.671957
C	0.855239	0.671470	1.218412
C	-0.904549	-0.680074	-0.828960
C	-1.435999	0.578967	-0.513023
C	0.733703	2.386393	-1.100337
C	2.032492	-1.441498	1.258155
H	2.208086	-2.429433	0.837999
C	-2.742425	0.885784	-0.897672
H	-3.153812	1.858269	-0.638044
C	-1.681684	-1.584579	-1.567095
H	-1.273818	-2.561118	-1.819125
C	1.414416	2.778842	-2.020522
H	2.019502	3.105500	-2.837091
C	-2.966672	-1.249083	-1.963863
H	-3.550327	-1.966134	-2.533691
C	1.568175	1.059337	2.354395
H	1.384871	2.042596	2.781110
C	-3.513469	-0.013582	-1.622674
H	-4.522912	0.245942	-1.924078
C	2.748369	-1.026747	2.370126
H	3.486208	-1.693786	2.806193
C	2.515066	0.225558	2.935202
H	3.067624	0.547969	3.811547
H	0.630840	-2.001213	-0.727012

Thermodynamic properties (298.15 K): *ZPE* = 492.57 kJmol^{-1}, H^o = –2829.445700 au, S^o = 454.09 Jmol^{-1}K^{-1}, G^o = –2829.497267, C_v = 234.12 Jmol^{-1}K^{-1}.

Table **S13** Allowed transitions for electronic spectra of **4**. (ωBP97X-D/6-31G*)

nm	Strength	Transition	%
209.7	0.0296	HOMO → LUMO+3	44
		HOMO-1 → LUMO+1	34
211.5	0.0560	HOMO → LUMO+4	69
221.8	0.0139	HOMO-1 → LUMO	57
		HOMO-1 → LUMO+4	15
235.5	0.2048	HOMO → LUMO+2	65
256.6	0.0814	HOMO → LUMO+1	79
260.2	0.1115	HOMO → LUMO	85

(f) HC≡CAsC_4H_4 (5')

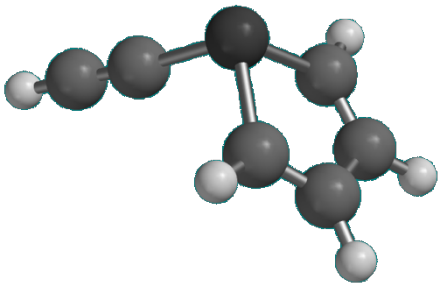

Figure S13. Optimised geometry for **5'** (ωBP97X-D/6-31G*)

Table S14. Cartesian Coordinates for HC≡CAsC_4H_4 (**5'**)

Atom	x	y	z
C	-0.477428	-1.325361	-0.490025
H	-0.555070	-2.397577	-0.336582
C	0.057862	-0.737767	-1.573293
H	0.484394	-1.294480	-2.407462
C	0.058338	0.738386	-1.573484
H	0.484788	1.294687	-2.408000
C	-0.475798	1.325884	-0.489626
H	-0.554145	2.398215	-0.337411
As	-1.270181	0.000657	0.680639
C	0.021632	-0.000783	2.066229
C	0.769056	-0.000916	3.017764
H	1.444894	-0.000946	3.847534

Thermodynamic properties (298.15 K, ωBP97X-D/cc-PVTζ): *ZPE* = 211.36 kJmol^{-1}, H^o = –2467.004640 au, S^o = 356.02 Jmol^{-1}K^{-1}, G^o = –2467.045069, C_v = 114.24 Jmol^{-1}K^{-1}.

Table S15 Allowed transitions for electronic spectra for **5'**. (ωBP97X-D/cc-PVTζ)

nm	Strength	Transition	%
190.9	0.0186	HOMO-2 → LUMO+1	40
		HOMO-1 → LUMO+2	37
206.0	0.0088	HOMO-2 → LUMO	77
206.3	0.0071	HOMO → LUMO+1	57
213.8	0.0306	HOMO-1 → LUMO+1	64
250.7	0.0296	HOMO → LUMO	79
252.3	0.0486	HOMO-1 → LUMO	94

Selection of Density Functional and Basis Sets - To assess the possible limitations in employing the economic ωBP97X-D/6-31G*/LANL2Dζ level of theory here, the model complex [W(CAsC$_4$H$_4$)(CO)$_2$(Tp)](**3'**) was also interrogated at the ωB97X-D/6-311+G(2df,2p)/Def2-TzVPPD(W) level of theory. The latter is a triple-zeta basis set with two sets of d-type and one set of f-type polarization functions in addition to a set of diffuse functions on non-hydrogen atoms and two sets of p-type polarisation functions on hydrogen atoms. This is used in conjunction with the Def2-TζVPPD basis set and associated pseudopotential for tungsten. The ωBP97X-D functional (RSH-GGA) was chosen due to its consideration of long-range non-bonded dispersion effects. Figure S14 presents the near identical energies and topologies of the frontier orbitals of interest derived at the two levels of theory suggesting that the faster ωBP97X-D/6-31G*/LANL2Dζ(W) methodology is sufficient for the present qualitative discussion of bonding within these heterocyclic carbyne complexes.

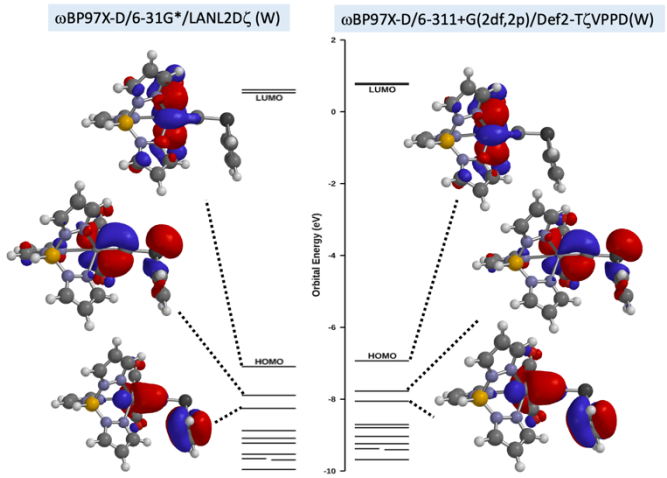

Figure S14. Comparison of energies and topologies of the frontier orbitals of interest derived at the

Mechanistic Conjecture: Conversion of 3 to 4

NB: The refinement of the molecular model for **4** was performed with the two arsenic centres being separated by either an oxygen atom or a methylene group. Given the limited quality of the data set, it is not surprising that the residuals did not adequately differentiate between O and CH_2. The following mechanistic conjecture assumes the latter and whilst it is completely unsubstantiated, we consider it to be a plausible route for the formation of **4**.The key, unprecedented step involves 1,2 migration of the alkylidynyl unit around the arsolyl ring to generate a tautomeric alkenylarsine that then undergoes nucleophilic attack by ethanol/ethoxide to afford an arsenide nucleophile. The nature of the bridging group between the two arsenic atoms therefore depends on whether oxidation (O) occurs followed by condensation or alternatively (CH_2) whether the arsenide undergoes nucleophilic attack with the solvent CH_2Cl_2 (Scheme S1).

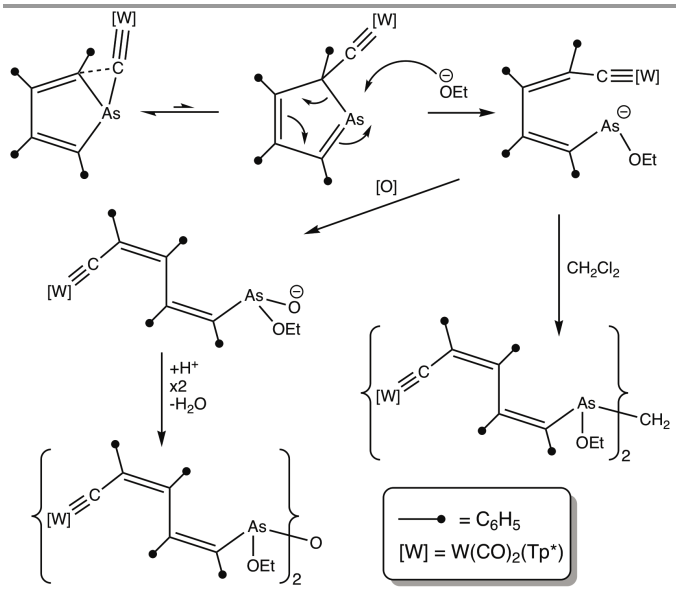

Scheme S1. Mechanistic conjecture to account for the formation of {(Tp*)(CO)$_2$W≡C-(CPh)$_4$As(OEt)}$_2$A (A = O, CH_2).

Notes and References

1 CrysAlis PRO, Agilent Technologies Ltd, Yarnton, Oxfordshire, England, 2014.

2 D. Aragão, J. Aishima, H. Cherukuvada, R. Clarken, M. Clift, N. P. Cowieson, D. J. Ericsson, C. L. Gee, S. M. Mudie, S. Panjikar, J. R. Price, A. Riboldi-Tunnicliffe, R. Rostan, R. Williamson and T. T. Caradoc-Davies, *J. Synchr. Rad.*, 2018, **25**, 885–891.

3 T. M. McPhillips, S. E. McPhillips, H.-J. Chiu, A. E. Cohen, A. M. Deacon, P. J. Ellis, E. Garman, A. Gonzalez, N. K. Sauter, R. P. Phizackerley, S. M. Soltis and P. Kuhn, *J. Synchr. Rad.*, 2002, **9**, 401-406.

4 W. Kabsch, *J. Appl. Crystallogr.*, 1993, **26**, 795-800.

5 (a) G. Sheldrick, *Acta Crystallogr. Sect. A: Found. Crystallogr.*, 2008, **64**, 112-122; (b) G. M. Sheldrick, *Acta Crystallogr. Sect. C: Cryst. Struct. Commun.*, 2015, **71**, 3-8.

6 (a) C. F. Macrae, P. R. Edgington, P. McCabe, E. Pidcock, G. P. Shields, R. Taylor, M. Towler and J. van de Streek, *J. Appl. Crystallogr.*, 2006, **39**, 453-457; (b) C. F. Macrae, I. J. Bruno, J. A. Chisholm, P. R. Edgington, P. McCabe, E. Pidcock, L. Rodriguez-Monge, R. Taylor, J. van de Streek and P. A. Wood, *J. Appl. Crystallogr.*, 2008, **41**, 466-470.

7 (a) T. Desmond, F. J. Lalor, G. Ferguson and M. Parvez, *J. Chem. Soc., Chem. Commun.*, 1983, 457-459; (b) F. J. Lalor, T. J. Desmond, G. M. Cotter, C. A. Shanahan, G. Ferguson, M. Parvez and B. Ruhl, *J. Chem. Soc., Dalton Trans.*, 1995, 1709-1726; (c) A. L. Colebatch and A. F. Hill, *J. Am. Chem. Soc.*, 2014, **136**, 17442-17445.

8 (a) A. Reinholdt, J. Bendix, A. F. Hill and R. A. Manzano, *Dalton Trans.*, 2018, **47**, 14893-14896; (b) B. J. Frogley, A. F. Hill, R. Shang, M. Sharma and A. C. Willis, *Chem. Eur. J.*, 2020, **26**, 8819-8827.

9 R. Uson, A. Laguna, M. Laguna , D. A. Briggs , H. H. Murray and J. P. Fackler Jr, in *Inorg. Synth.*, ed. H. D. Kaesz, 1989, vol. **26**, ch. 17, pp. 85-91.

10 S. C. Sendlinger, B. S. Haggerty, A. L. Rheingold and K. H. Theopold, *Chem. Ber.*, 1991, **124**, 2453-2456.

11 *Spartan 18*® (2018) Wavefunction, Inc., 18401 Von Karman Ave., Suite 370 Irvine, CA 92612 U.S.A

12 J.-D. Chai and M. Head-Gordon, *J. Chem. Phys.*, 2008, **128**, 0841061–18410615; (*b*) J.-D. Chai and M. Head-Gordon, *Phys. Chem. Chem. Phys.*, 2008, **10**, 6615– 6620.

13 (a) P. J. Hay and W.R. Wadt, *J. Chem. Phys.*, 1985, **82**, 270-283. (b) W. R. Wadt and P. J. Hay, *J. Chem. Phys.* 1985, **82**, 284-298. (c) P. J. Hay, W. R. Wadt, *J. Chem. Phys.,* 1985, **82**, 299-310.

14 W. J. Hehre, R. Ditchfeld and J. A. Pople, *J. Chem. Phys.*, 1972, **56**, 2257-2261

15 B. J. Frogley and A. F. Hill, *Chem. Commun.*, 2018, **54**, 2126-2129.

16 G. M. Jamison, A. E. Bruce, P. S. White and J. L. Templeton, *J. Am. Chem. Soc.*, 1991, **113**, 5057-5059.

17 M. R. St.-J. Foreman, A. F. Hill, A. J. P. White and D. J. Williams, *Organometallics*, 2003, **22**, 3831-3840.

18 https://cccbdb.nist.gov/vibscalejust.asp

19 M. D. Halls, J. Velkovski and H. B. Schlegel *Theor. Chem. Acc*. 2001, **105**, 413-421.

Selected Spectra

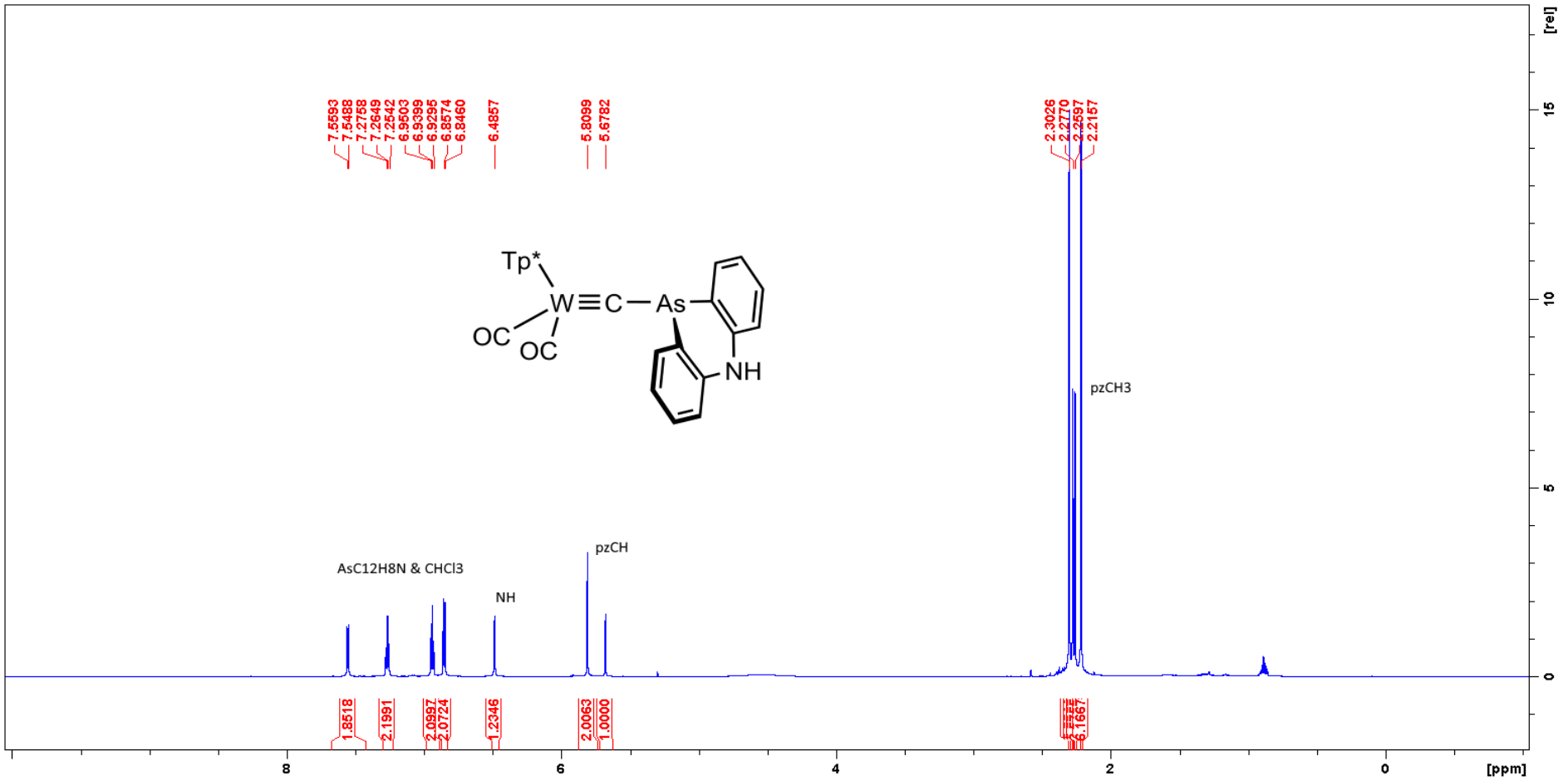

Figure S15. ^{1}H NMR Spectrum (700 MHz, CDCl3, 25 ˚C, δ) of [W(≡CAs$C_{12}H_8$NH)$(CO)_2$(Tp*)] (**2**).

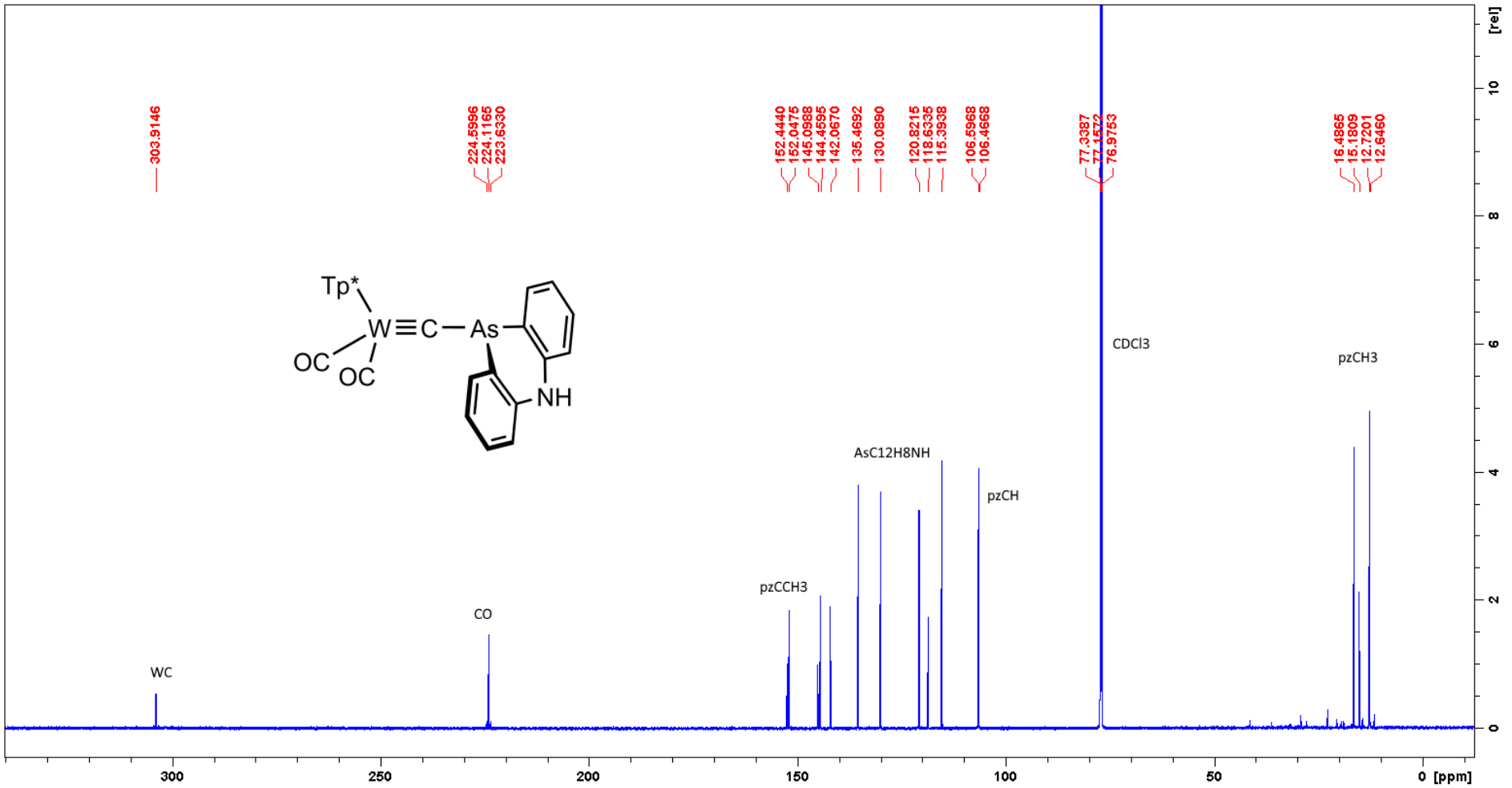

Figure S16. $^{13}C\{^{1}H\}$ NMR Spectrum (176 MHz, $CDCl_3$, 25 ˚C, δ) of [W(≡CAs$C_{12}H_8$NH)$(CO)_2$(Tp*)] (**2**).

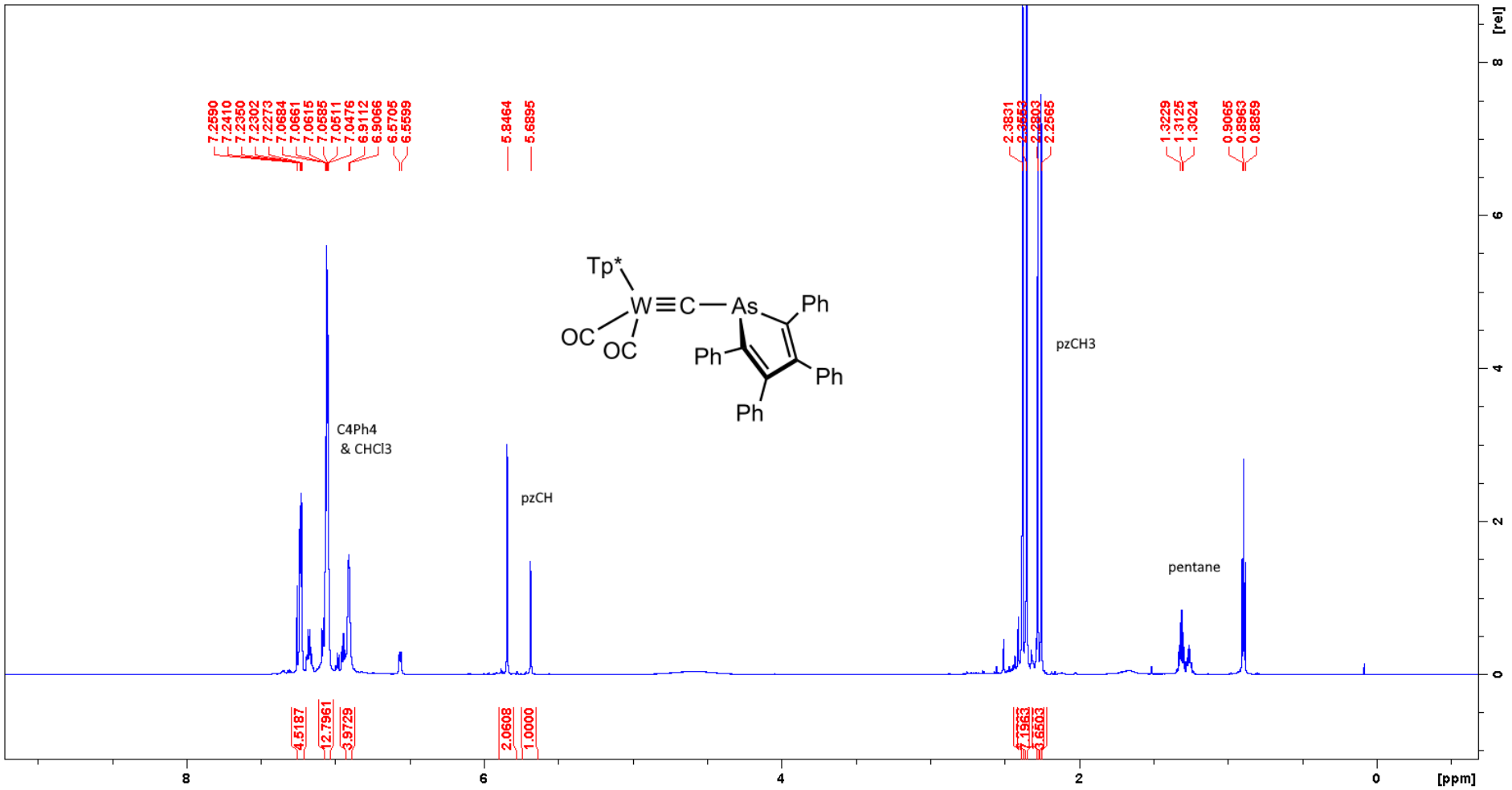

Figure S17. ^{1}H NMR Spectrum (700 MHz, $CDCl_3$, 25 ˚C, δ) of [W(≡CAsC_4Ph_4)$(CO)_2$(Tp*)] (**3**)

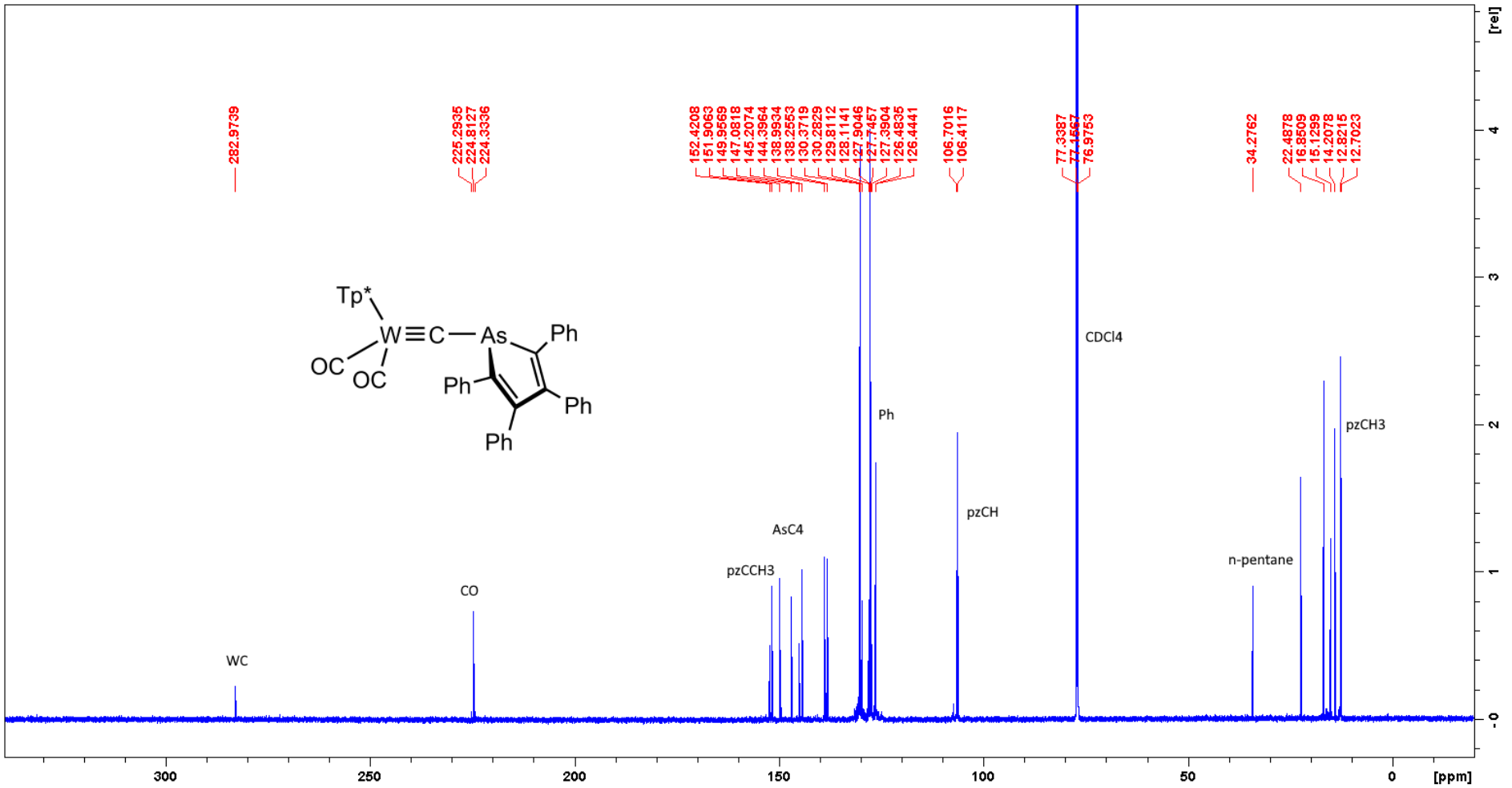

Figure S18. $^{13}C\{^{1}H\}$ NMR Spectrum (176 MHz, $CDCl_3$, 25˚C, δ) of $[W(\equiv CAsC_4Ph_4)(CO)_2(Tp^*)]$ (**3**)

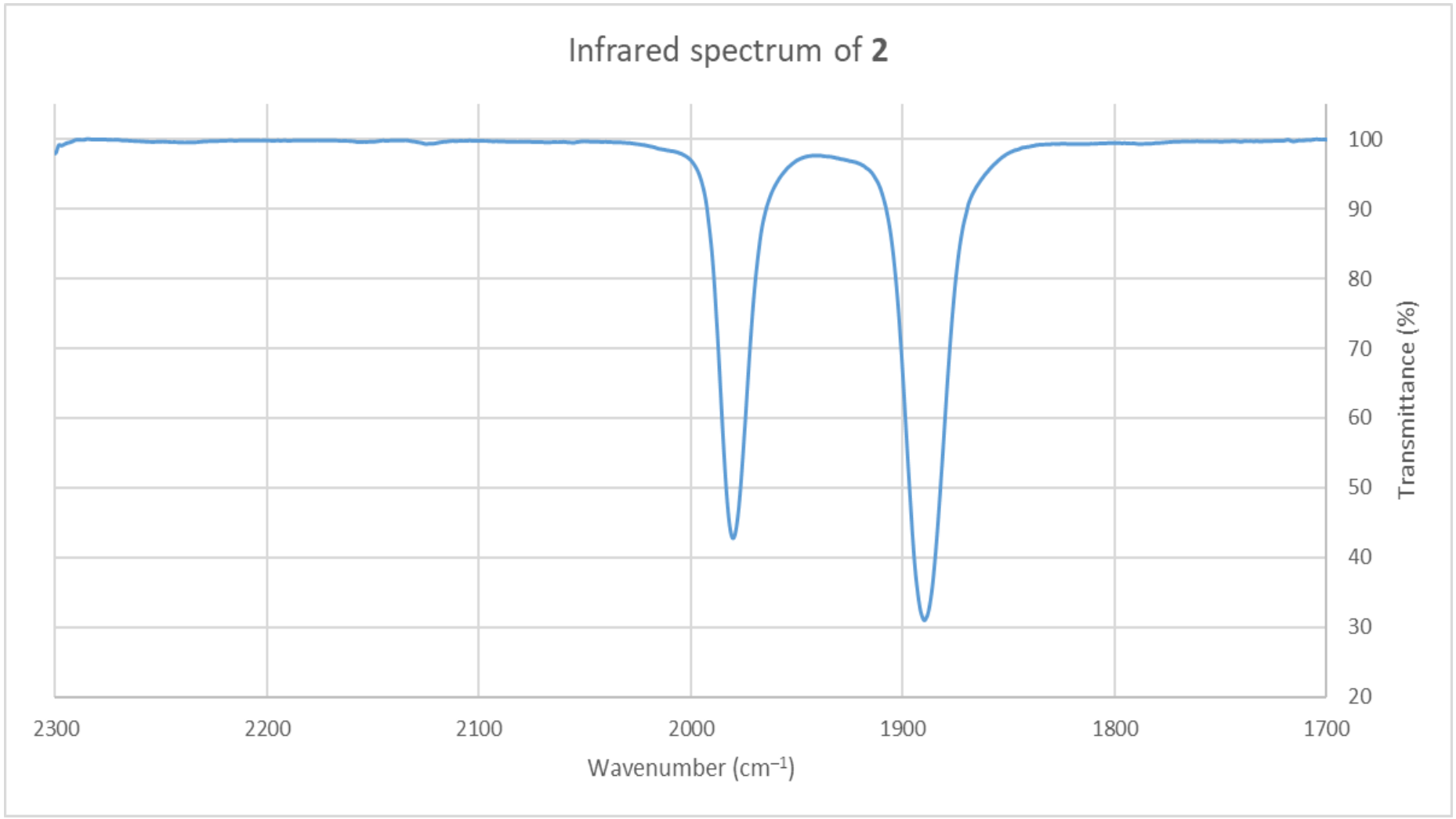

Figure S19. Infrared spectrum (CH_2Cl_2, cm^{-1}) of [W(≡CAs$C_{12}H_8$NH)$(CO)_2$(Tp*)] (**2**).

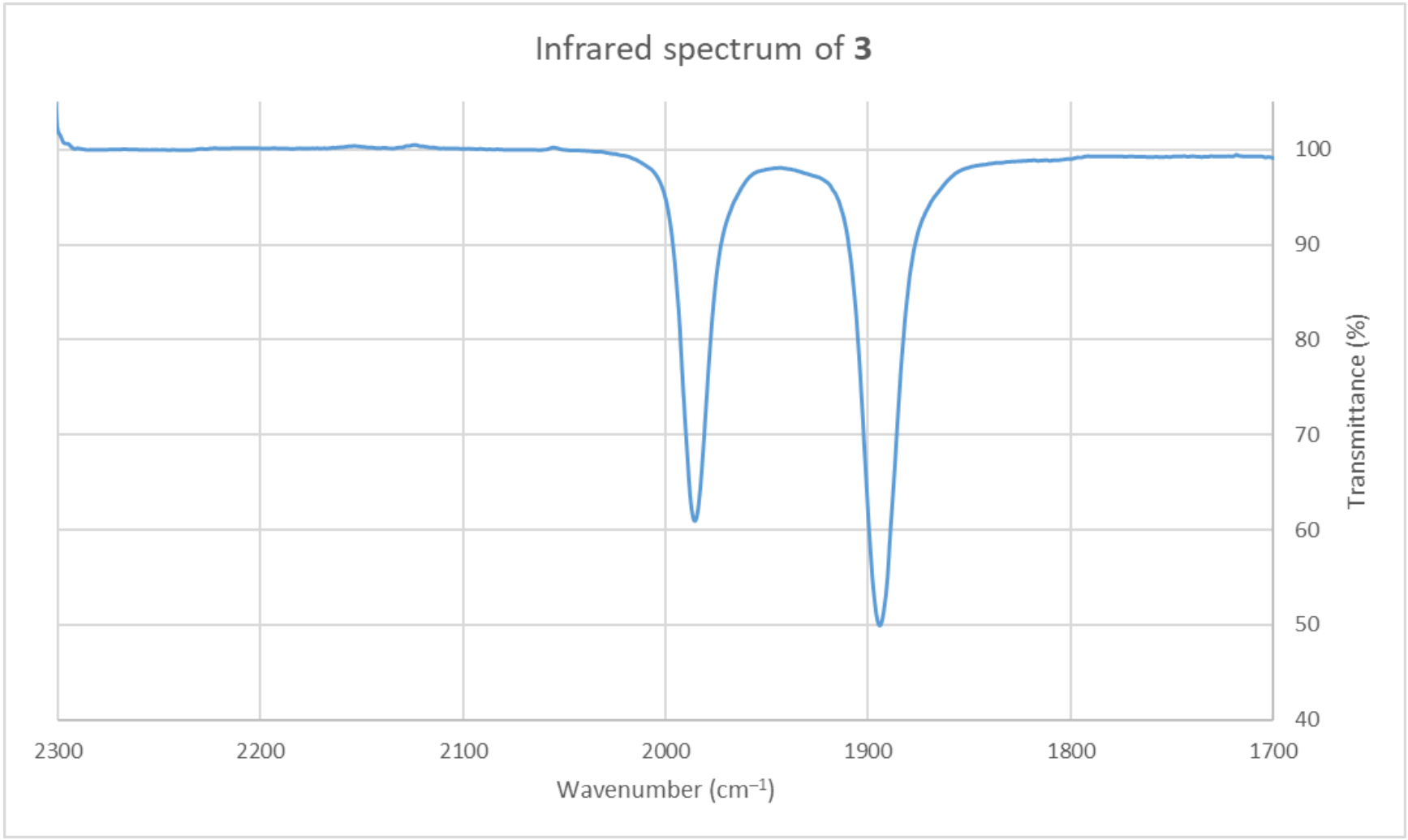

Figure S20. Infrared spectrum (CH_2Cl_2, cm^{-1}) of [W(≡CAsC_4Ph_4)$(CO)_2$(Tp*)] (**3**).

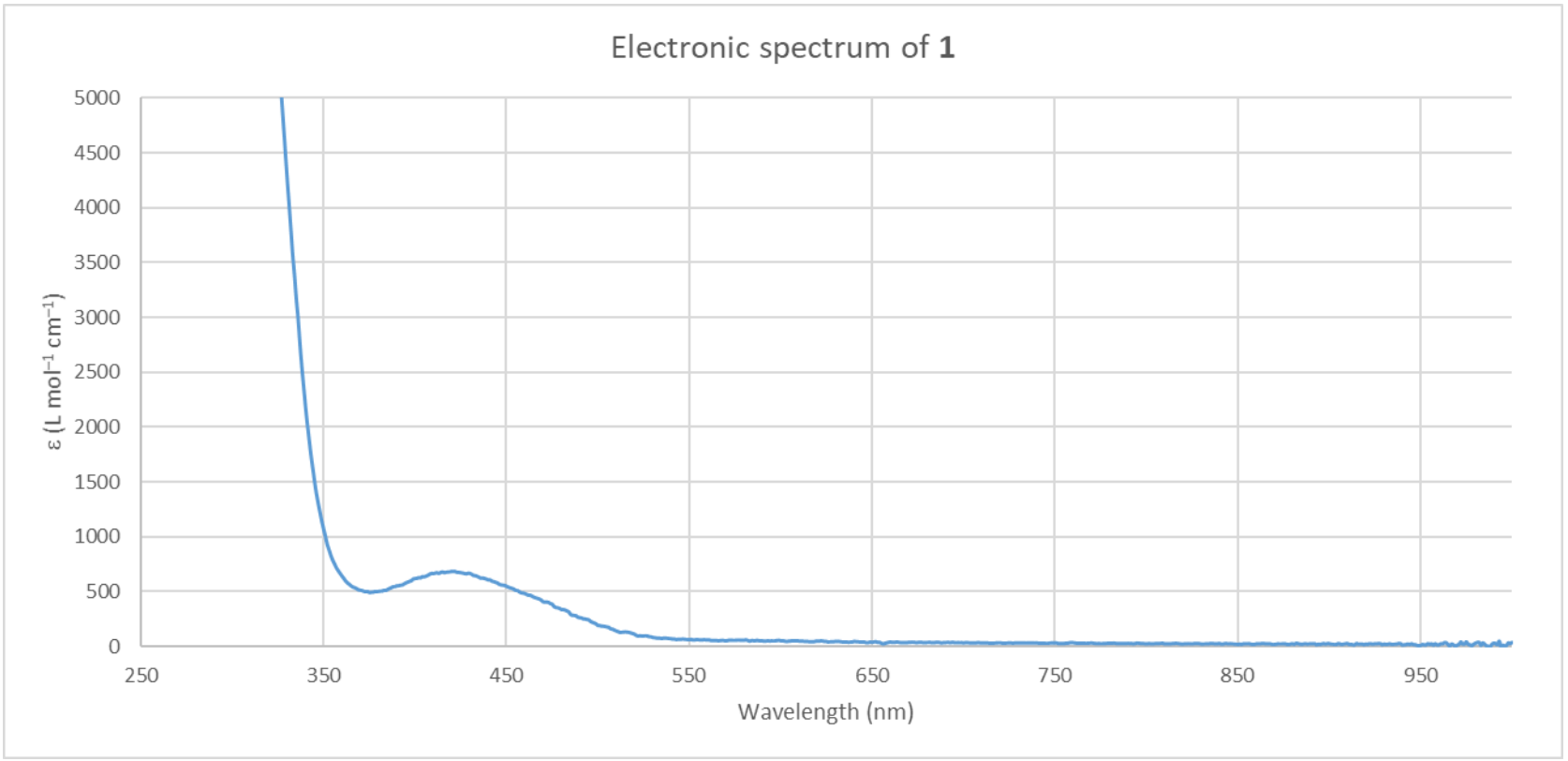

Figure S21. Electronic spectrum (CH_2Cl_2) of [W(≡CAsPh_2)$(CO)_2$(Tp*)] (**1**) (2.4 x 10^{-4} M).

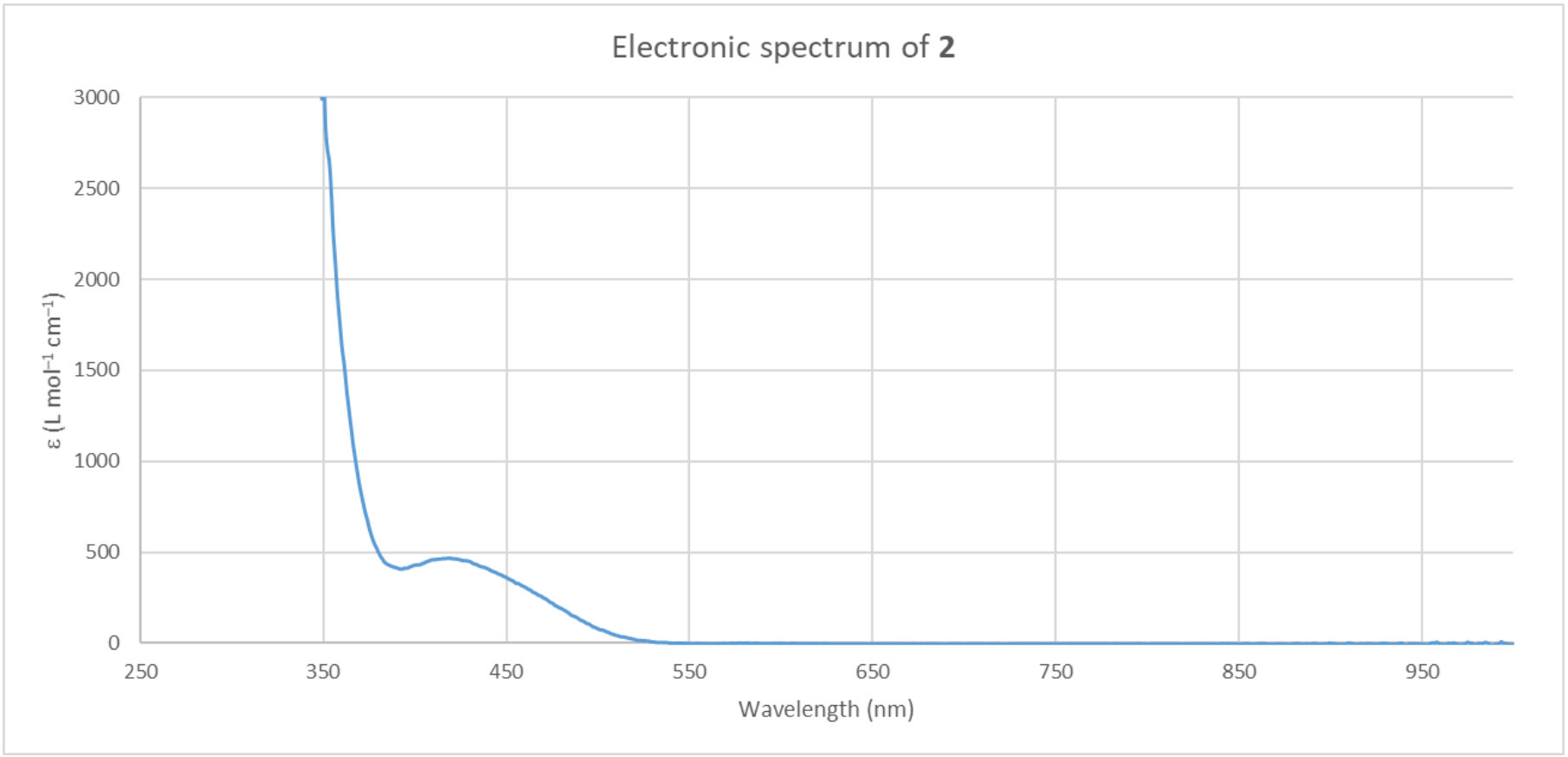

.

Figure S22. Electronic spectrum (CH_2Cl_2) of [W(≡CAs$C_{12}H_8$NH)$(CO)_2$(Tp*)] (**2**) (6.6 x 10^{-4} M)

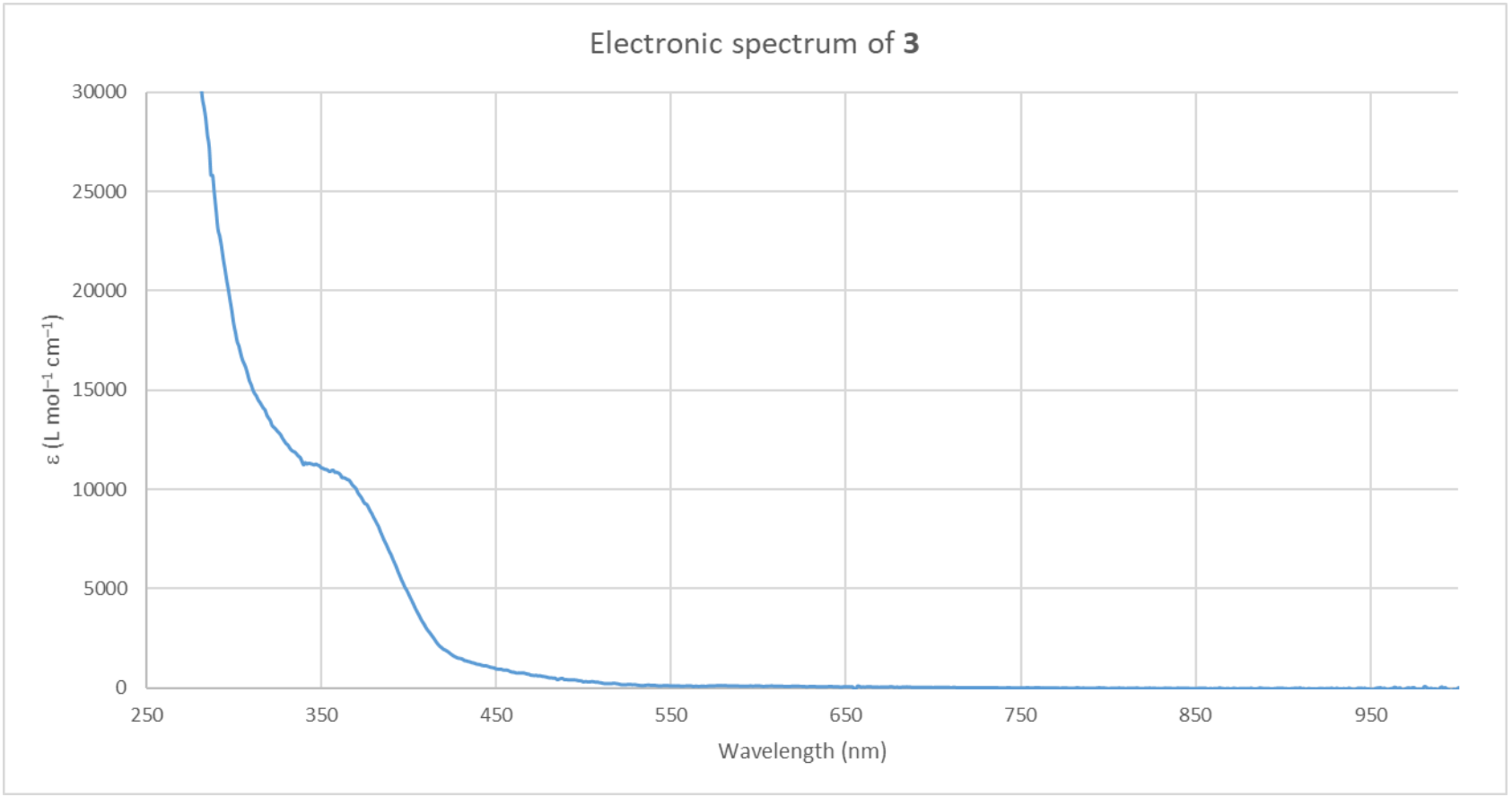

Figure S23. Electronic spectrum (CH_2Cl_2) of [W(≡CAsC_4Ph_4)$(CO)_2$(Tp*)] (**3**) (6.8 x 10^{-5} M).

Alkynes

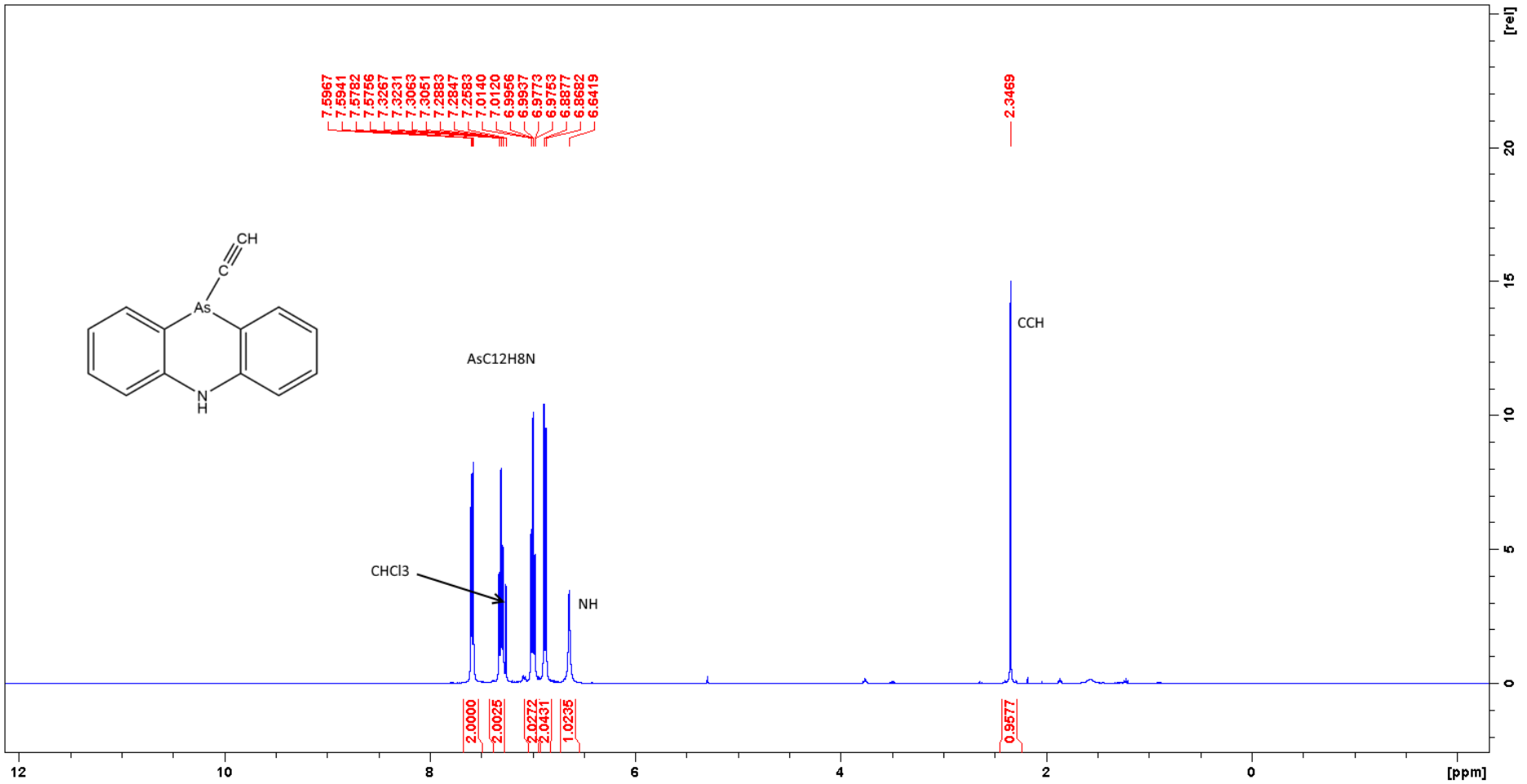

Figure S24. ^{1}H NMR Spectrum (700 MHz, $CDCl_3$, 25 ˚C, δ) of $HC{\equiv}CAs(C_6Ph_4)_2NH$ (**4**)

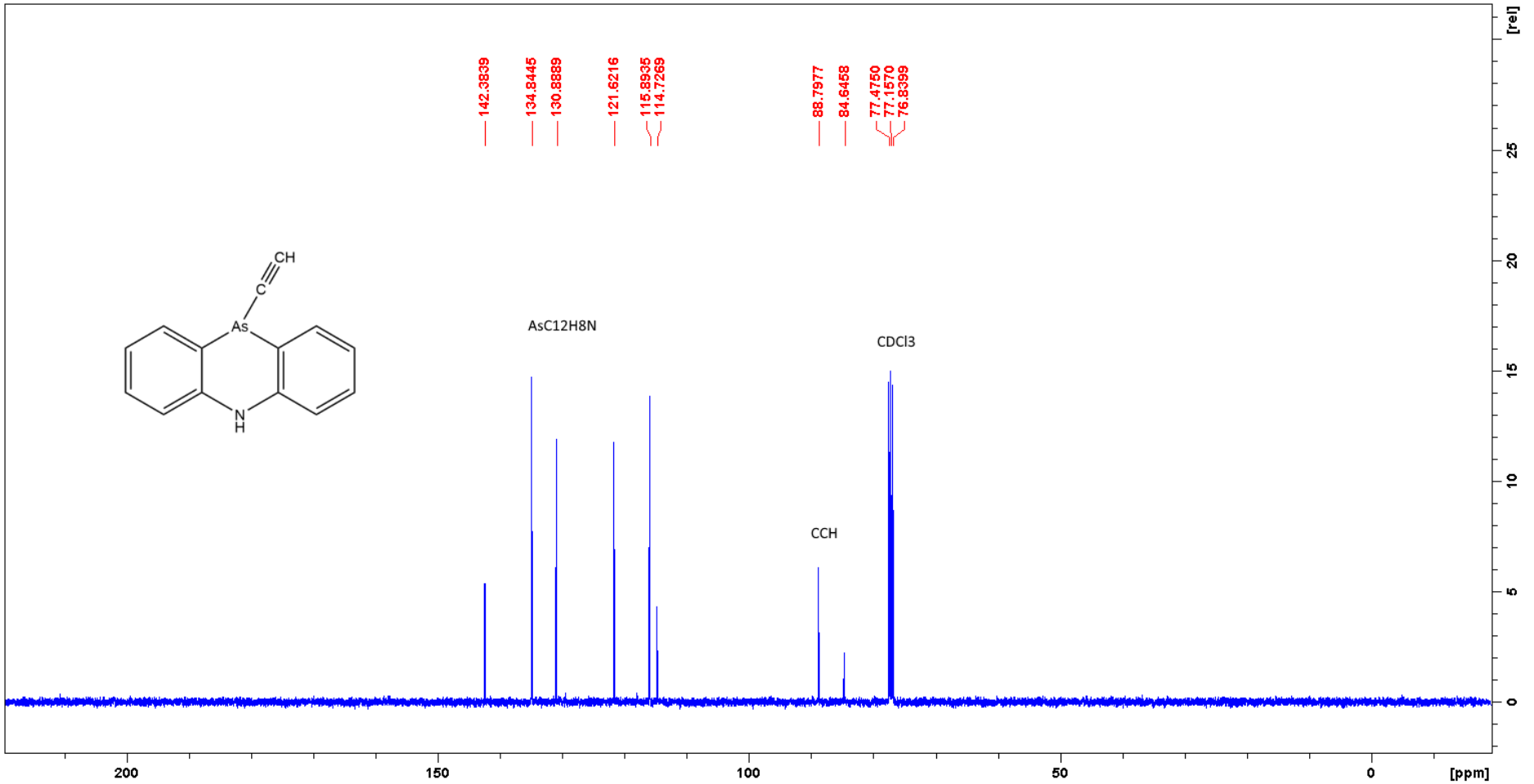

Figure S25. $^{13}C\{^{1}H\}$ NMR Spectrum (101 MHz, $CDCl_3$, 25 ˚C, δ) of $HC{\equiv}CAs(C_6Ph_4)_2NH$ (**4**)

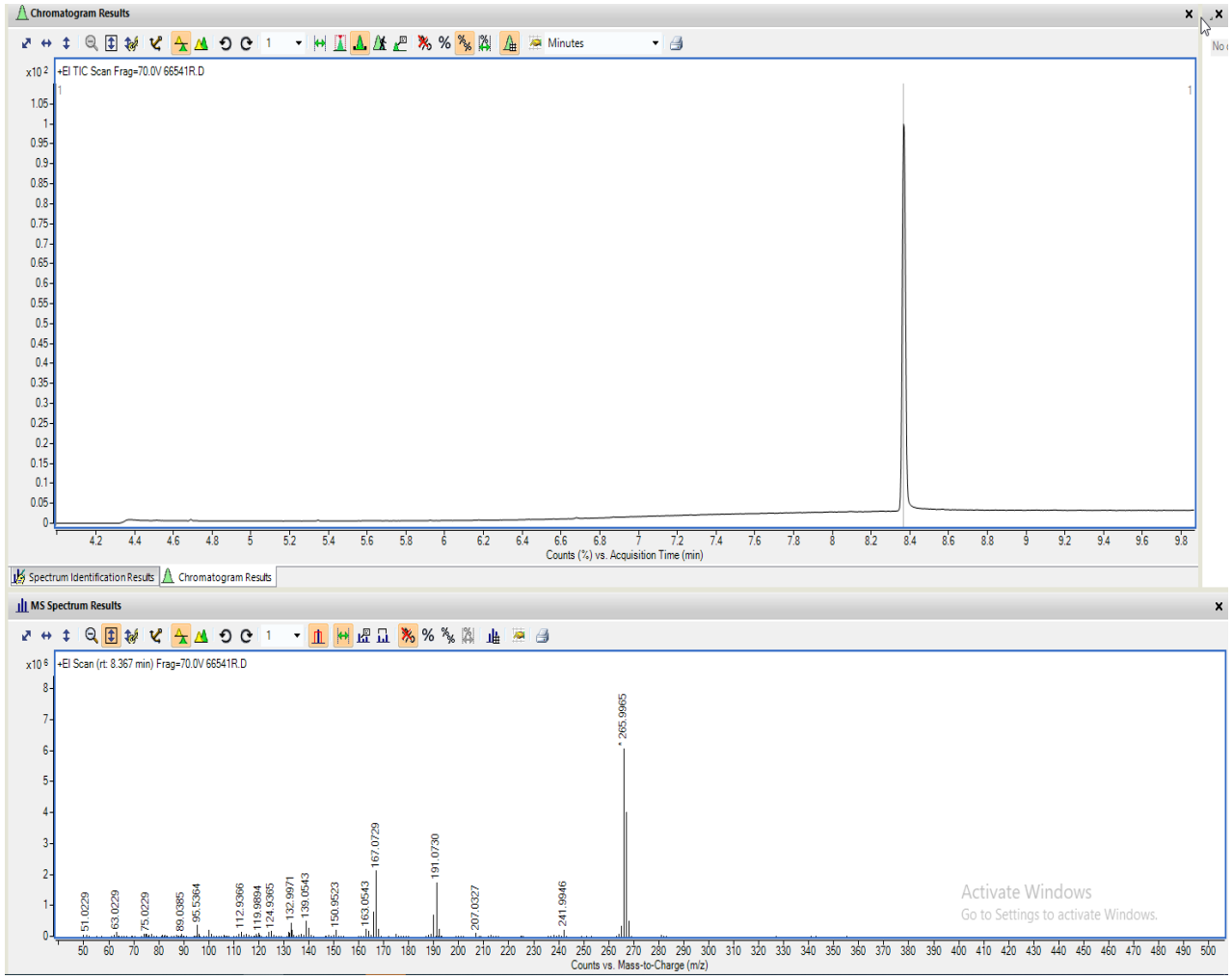

Figure S26. EI GC-MS Spectrum of HC≡CAs(C_6Ph_4)$_2$NH (**4**)

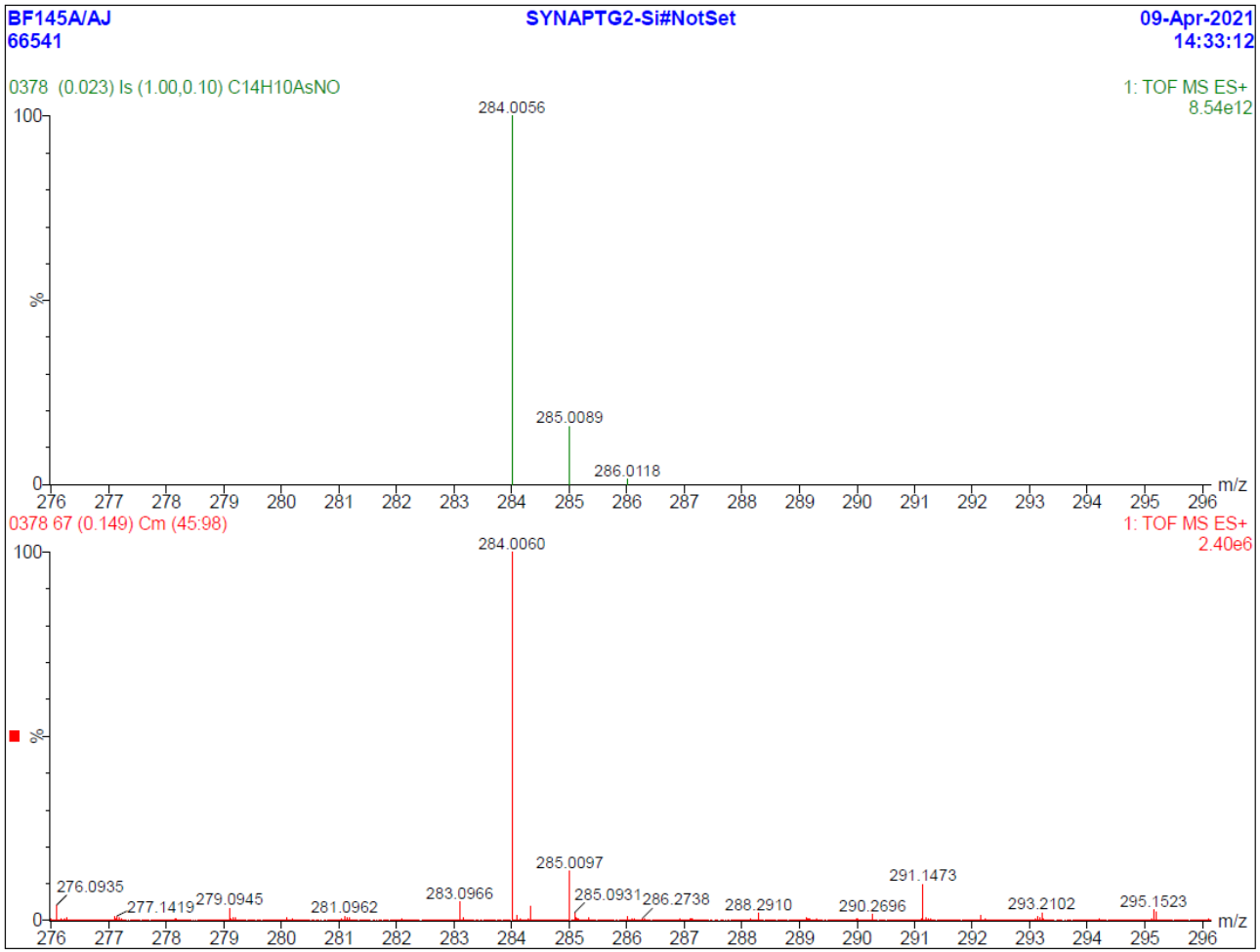

Figure S27. ESI-MS of HC≡CAs$(C_6H_4)_2$NH (**4**)

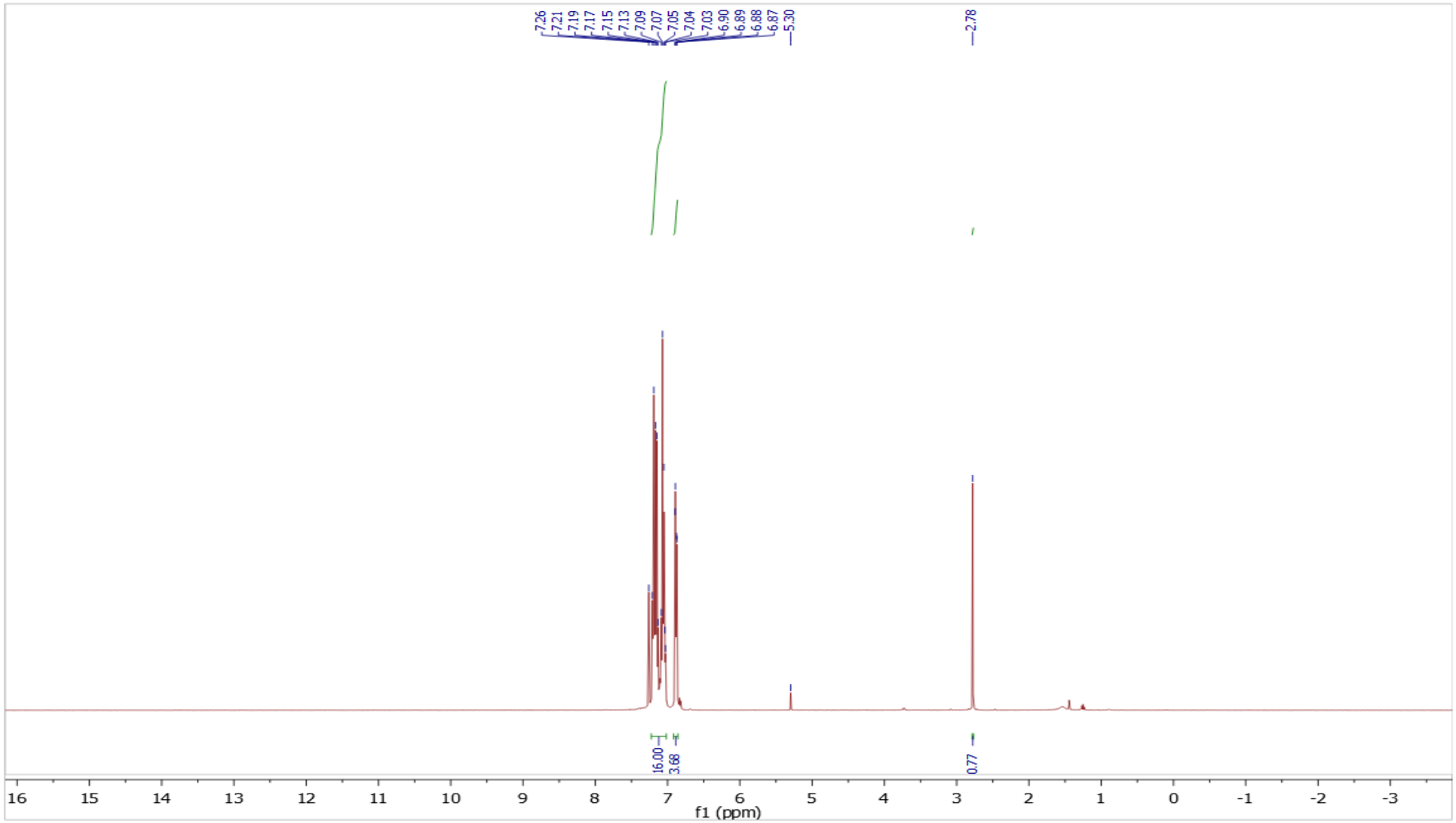

Figure S28. ^{1}H NMR Spectrum (400 MHz, $CDCl_3$, 25 ˚C, δ) of $HC{\equiv}CAsC_4Ph_4$ (**5**)

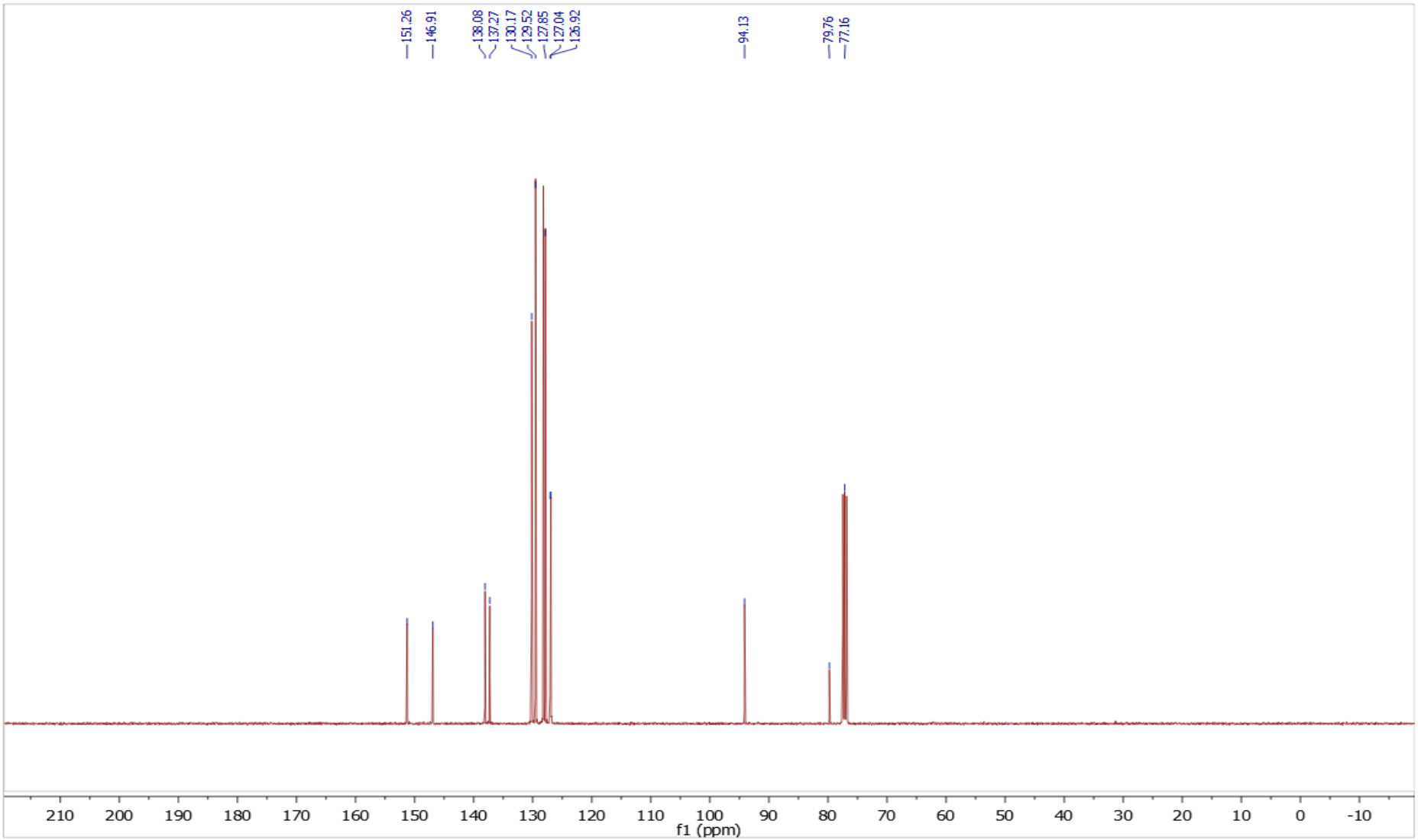

Figure S29. $^{13}C\{^{1}H\}$ NMR Spectrum (101 MHz, $CDCl_3$, 25 ˚C, δ) of $HC{\equiv}CAsC_4Ph_4$ (**5**)

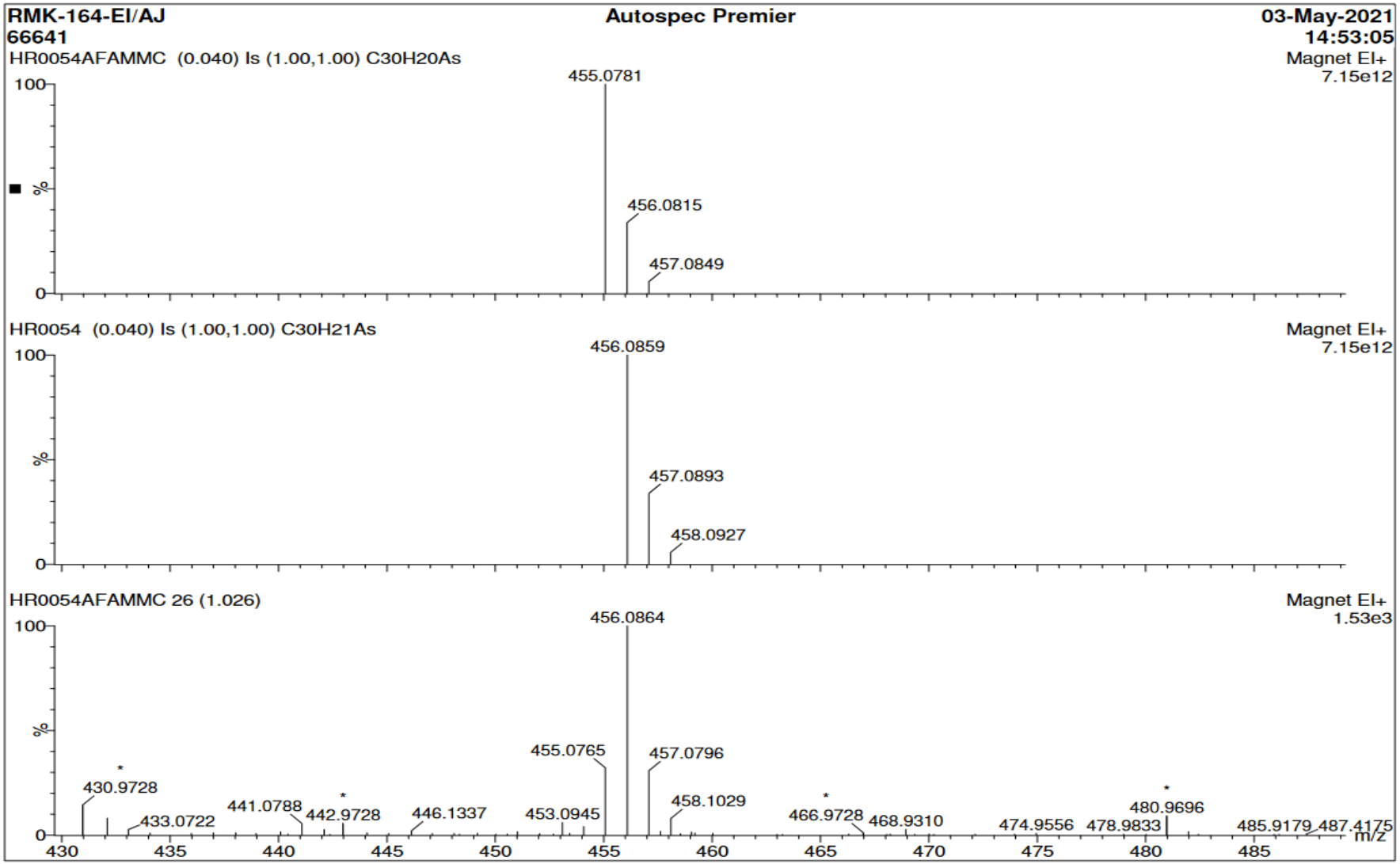

Figure S30. EI GC-MS of $HC{\equiv}CAsC_4Ph_4$ (**5**)

Figure S31. EI GC-MS of HC≡CAsC_4Ph_4 (**5**)